








ARTICLE

Cross-talk between the calcium channel TRPV4 and reactive oxygen species interlocks adhesive and degradative functions of invadosomes

Sanela Vellino¹, Christiane Oddou^{1*}, Paul Rivier^{1*}, Cyril Boyault¹, Edwige Hiriart-Bryant¹, Alexandra Kraut², René Martin³, Yohann Coute², Hans-Joachim Knölker³, Miguel A. Valverde⁴, Corinne Albigès-Rizo^{1**}, and Olivier Destaing^{1**}

Invadosomes support cell invasion by coupling both acto-adhesive and extracellular matrix degradative functions, which are apparently antagonistic. β 1-integrin dynamics regulate this coupling, but the actual sensing mechanism and effectors involved have not yet been elucidated. Using genetic and reverse genetic approaches combined with biochemical and imaging techniques, we now show that the calcium channel TRPV4 colocalizes with β 1-integrins at the invadosome periphery and regulates its activation and the coupling of acto-adhesive and degradative functions. TRPV4-mediated regulation of podosome function depends on its ability to sense reactive oxygen species (ROS) in invadosomes' microenvironment and involves activation of the ROS/calcium-sensitive kinase Ask1 and binding of the motor MYO1C. Furthermore, disease-associated TRPV4 gain-of-function mutations that modulate ECM degradation are also implicated in the ROS response, which provides new perspectives in our understanding of the pathophysiology of TRPV4 channelopathies.

Introduction

Numerous cell invasion processes rely on the ability to digest the basal membrane, which is supported by invadosomes. Invadosomes are acto-adhesive structures composed of an F-actin core surrounded by a ring of integrins and adhesion molecules that promote normal protrusions to the ECM (Labernadie et al., 2014). This acto-adhesive activity is dynamically coupled to the ability of the invadosome to locally digest the ECM. We refer to this coupling by the abbreviation ADC (acto-adhesion and degradation coupling). ECM degradation is sustained by the local exocytosis of activated MT1-MMP at the plasma membrane (Sakurai-Yageta et al., 2008; Branch et al., 2012). However, the physical or biochemical cues regulating ADC are poorly understood. Some studies have highlighted a few molecular mechanisms regulating this coupling, such as the phosphorylation of Tks4, the functional equilibrium between paxillin family members, the localized activation of Rac3 recruited by Ca²⁺-dependent calcium and integrin-binding protein 1 (CIB1), and the dynamics of activation of the tyrosine kinase SRC and β 1-integrins (Buschman et al., 2009; Destaing et al., 2010; Kelley

et al., 2010; Petropoulos et al., 2016; Donnelly et al., 2017). For these adhesive proteins, ADC is better supported by oscillation between active/inactive states than when these proteins are simply maintained in active conformations. However, the sensing mechanism linking all these molecular machineries is still unknown. Perturbation of Ca²⁺ signaling could fine-tune functional coupling in invadosomes. Indeed, the nonspecific perturbation of Ca²⁺ entry decreases invadosome formation (Siddiqui et al., 2012; Nagasawa and Kojima, 2012). Moreover, pharmacological inhibition of store-operated calcium entry reduces invadosome formation and seems to also reduce the degradative activity of invadosomes (Sun et al., 2014). These observations led us to consider the functions of other Ca²⁺-specific channels in the sensing and regulation of ADC.

In addition, to confirm the importance of Ca²⁺ in invadosome functions, elucidating which of the numerous structurally different Ca²⁺ ion channels are implicated in different adhesion responses remains challenging. Indeed, the roles of specific Ca²⁺ channels associated with invadosomes and their downstream

¹Dynamique des systèmes d'adhérence, Institut for Advanced Biosciences, Centre de Recherche University Grenoble Alpes/INSERM U1209/Centre National de la Recherche Scientifique Unité mixte de recherche 5309, La Tronche, France; ²Laboratoire EDyP, Institute of Biosciences and Biotechnologies of Grenoble-Biologie à Grande Echelle, Commissariat à l'Énergie Atomique Grenoble, Grenoble, France; ³Faculty of Chemistry, Technische Universität Dresden, Dresden, Germany; ⁴Laboratory of Molecular Physiology, Department of Experimental and Health Sciences, Universitat Pompeu Fabra, Barcelona, Spain.

*C. Oddou and P. Rivier contributed equally to this paper; **C. Albigès-Rizo and O. Destaing contributed equally to this paper; Correspondence to Olivier Destaing: olivier.destaing@univ-grenoble-alpes.fr.

© 2021 Vellino et al. This article is distributed under the terms of an Attribution–Noncommercial–Share Alike–No Mirror Sites license for the first six months after the publication date (see <http://www.rupress.org/terms/>). After six months it is available under a Creative Commons License (Attribution–Noncommercial–Share Alike 4.0 International license, as described at <https://creativecommons.org/licenses/by-nc-sa/4.0/>).

signaling pathways in multiple integrin-based adhesion processes are currently poorly understood. To date, only the cationic channels transient receptor potential melastatin subfamily member 7 (TRPM7; Clark et al., 2006), TRPV2 (Nagasawa and Kojima, 2012), and Piezo2 (Pardo-Pastor et al., 2018) have been implicated in the regulation of invadosomes or invasion. β 1-integrins are key regulators of invasion, as they are essential for the formation and activation of different models of invadosomes (Destaing et al., 2010; Poincloux et al., 2011; Beaty et al., 2013), and the specific relationship of β 1-integrins with calcium channel TRPV4 led us to investigate its function in invadosomes. Indeed, TRPV4 is localized at the plasma membrane, sensitive to mechanical modulation, and ultra-rapidly gated following β 1-integrin activation (Matthews et al., 2010). Modulation of TRPV4 ion permeation by physiological stimuli is sufficient to regulate focal adhesion size and cell force production at the rear edge of migrating cells (Mrkonjić et al., 2015). Moreover, the invadosome-derived sealing zone should be partially controlled by TRPV4 since the bone digestive activity of TRPV4^{-/-} osteoclasts is highly decreased (Masuyama et al., 2012).

The observed importance of mechano/osmosensitive ion channels (transient receptor potential melastatin subfamily member 7, Piezo2, and TRPV4) in adhesion structures raises a question about the nature of the stimuli they sense and the specificity of their downstream Ca²⁺-dependent signaling pathways in the regulation of these dynamic structures. TRPV4 is broadly expressed, polymodally gated, and sensitive to osmotic, mechanical, thermal, and chemical cues (Moore and Liedtke, 2017). Interestingly, some TRPVs (e.g., TRPV1 and TRPV4) are also sensitive to reactive oxygen species (ROS) production and signaling (Kishimoto et al., 2011; Kozai et al., 2014; Hong et al., 2016). The discovery of 70 mutations within the TRPV4 channel leading to severe skeletal and neuromuscular diseases calls for improved understanding of new aspects of its biology (White et al., 2016).

Based on the functional link between β 1-integrin and TRPV4, we investigated TRPV4-specific functions involved in the coupling of ADC activities in invadosomes. In addition to the specific accumulation of β 1-integrin and TRPV4 at the outer rim of invadosomes, the specific role of TRPV4 in ADC through its ability to assemble specific biochemical complexes controlled by localized Ca²⁺ entry was shown through combined genetic and reverse genetic approaches. TRPV4 mutants implicated in human diseases showed impaired ADC in invadosomes. Identification of TRPV4-binding partners revealed the substantial involvement of ROS-sensitive proteins such as ASK1 kinase. These results led us to investigate ROS sensing and signaling in ADC. By combining Ca²⁺ and ROS live imaging, we report that ROS participates in ADC through the modulation of TRPV4 activity. This ROS-dependent regulatory activity of TRPV4 is bidirectional, since it is supported by either extracellular or intracellular stretches of cysteines. This work provides new molecular evidence to describe how ADC is regulated through synergic ROS and Ca²⁺ signaling and opens a new direction in the field of invadosomes and clinical approaches to TRPV4 channelopathies.

Results

TRPV4 at the invadosome periphery sustains normal ADC

To test the functional role of TRPV4 in invadosomes, we first determined TRPV4 localization at the invadosome ring. tagRFP (TgRFP)-TRPV4^{WT} and LifeAct-GFP were coexpressed in mouse embryonic fibroblasts (MEF) cells stably expressing the constitutively active Src mutant SrcY527F (mouse embryonic fibroblast rc Y527F, MYF cells), leading to the formation of functional invadosomes (Destaing et al., 2010; Boateng and Huttenlocher, 2012; Petropoulos et al., 2016). TgRFP-TRPV4^{WT} was localized at the periphery of the invadosome ring (Fig. 1 a), reminiscent of β 1A-integrin localization in the invadosome, where other adhesive proteins such as paxillin-GFP and talin-GFP accumulated (Fig. S1, a and b). This localization was highly specific to TRPV4 and was not observed for other members of the TRP superfamily (its closest homologues TRPV1, TRPV2, TRPA1, TRPM5, and TRPM8; Fig. 1 a and Fig. S1 c). Live imaging of TgRFP-TRPV4^{WT} and the F-actin marker LifeAct-GFP revealed a significant association between an increase in TRPV4 and the disorganization of the invadosome ring (Fig. 1 b and Fig. S1 d).

To confirm the role of TRPV4 in invadosome disorganization, we investigated how the loss of endogenous TRPV4 affects invadosome functions. TRPV4 silencing in MYF cells increased the number, thickness, and average ring diameter of invadosome rings (Fig. 1 c) and at the same time decreased F-actin intensity (Fig. S1 e). To confirm these data, invadosomes were analyzed in MYF-TRPV4^{-/-} cells that did or did not stably reexpress TgRFP-TRPV4^{WT}. Consistent with the results of the TRPV4 silencing experiment, the rescued expression of TgRFP-TRPV4^{WT} in MYF-TRPV4^{-/-} cells significantly reduced the number, thickness, and average ring diameter of invadosomes (Fig. 1 d). siRNA experiments in MYF-TRPV4^{-/-} cells did not affect invadosome formation and confirmed the specificity of our silencing approach (Fig. S1, f and g).

The TRPV4-dependent modulation of invadosome thickness and ring diameter suggested possible changes in invadosome dynamics. Indeed, these structures have a lifespan of 2–20 min that can organize into round metastructures called rings through the coordinated assembly of new invadosome units at the outer rim and the disassembly of older invadosome units at the inner rim (Destaing et al., 2003). The rescued expression of TgRFP-TRPV4^{WT} in MYF-TRPV4^{-/-} cells increased the invadosome ring life span and thus slowed the displacement of invadosome rings, as measured by live imaging (Fig. S2 a). Indeed, the average invadosome ring life span in MYF-TRPV4^{-/-} mice did not exceed 15 min, while the reexpression of TgRFP-TRPV4^{WT} stabilized invadosome rings for >60 min (Fig. S2 a). Additionally, the overexpression of GFP-TRPV4^{WT} in MYF cells stabilized invadosome rings and increased their degradative activity (Fig. S2, b and c). Genetic and reverse genetic data clearly confirmed the importance of TRPV4 in regulating invadosome dynamics by regulating invadosome disassembly and stability.

Since TRPV4 clearly plays a role in the regulation of invadosome size and dynamics, we aimed to investigate whether TRPV4 also affects MT1-MMP-dependent ECM degradation. In addition, to induce the formation of large invadosomes, TRPV4

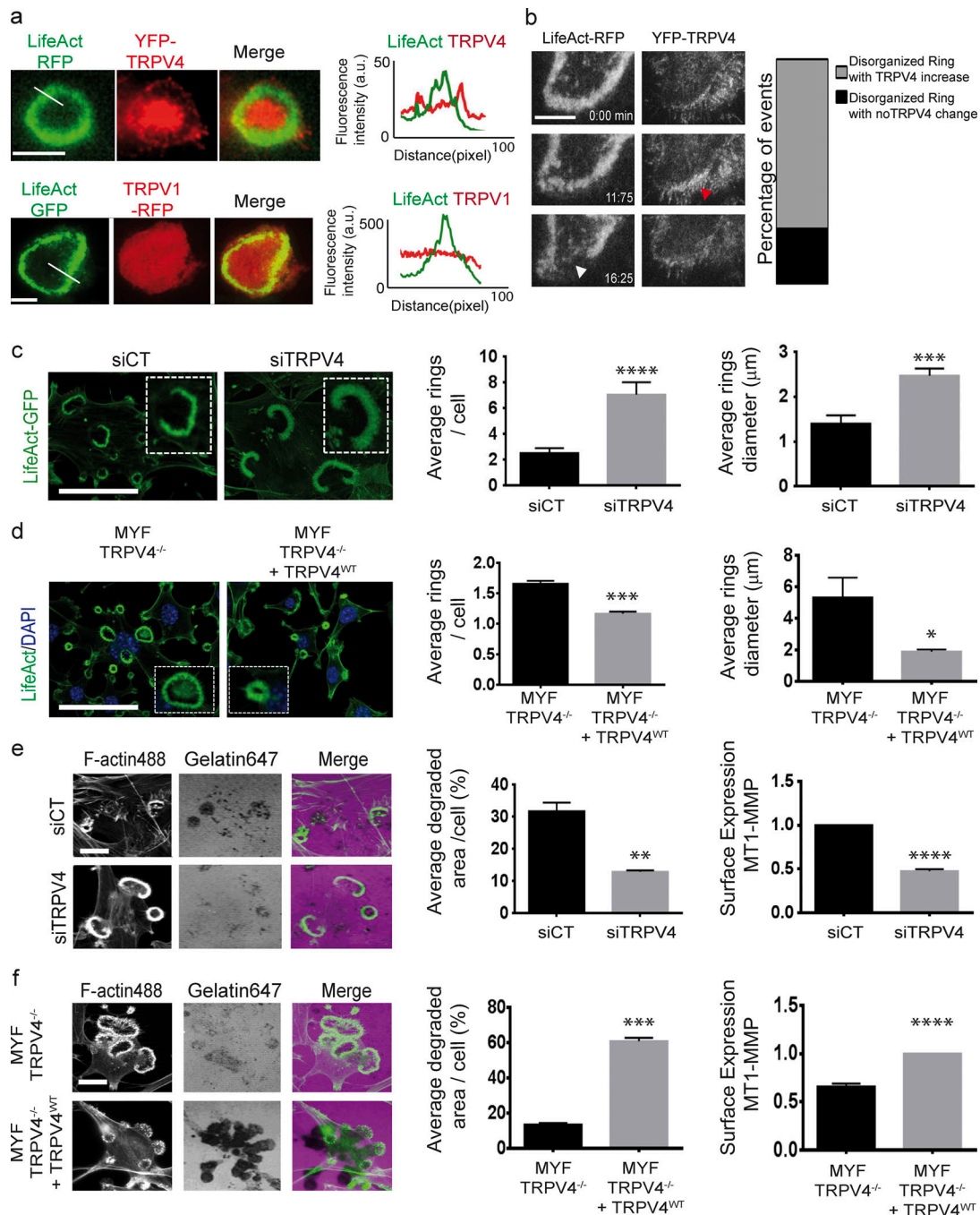


Figure 1. TRPV4 is an essential regulator of ADC in invadosomes. (a) Representative images of YFP-TRPV4 specifically accumulated at the periphery of invadosomes with its closest family member, TRPV1-RFP, in MYF cells expressing an invadosome marker (LifeAct fused to RFP or GFP). Analysis of the fluorescence intensity profile over the white lines indicating the invadosome thickness confirmed the specific accumulation of TRPV4 at the invadosome periphery. (b) Representative images extracted from a time series of MYF cells expressing LifeAct-RFP and YFP-TRPV4. The red arrowhead indicates YFP-TRPV4 accumulation that preceded invadosome disorganization (white arrowhead). The dynamics of 16 invadosomes were followed in order to determine that their disorganization was more correlated with an increase in TgRFP-TRPV4^{WT} at the invadosome periphery (75%, 12/16) than with no apparent change (25%, 4/16). (c) Representative images of MYF cells stably expressing LifeAct-GFP treated with control or TRPV4 siRNA (zoom on single invadosome ring in white boxes). TRPV4 silencing induced a significant increase in the number of invadosome rings per cell (SEM; $n = 3$; >100 cells per condition; unpaired t test) and thickness (SE; $n = 3$; >40 rings per condition; unpaired t test). (d) Representative images of MYF-TRPV4^{-/-} cells stably expressing LifeAct-GFP with or without TgRFP-TRPV4^{WT} (zoom on single invadosome ring in white boxes). Exogenous TgRFP-TRPV4^{WT} specifically decreased the formation of invadosome rings (SEM; $n = 3$; >100 cells per condition; unpaired t test) and their thickness (SEM; $n = 3$; >40 rings per condition; unpaired t test) in MYF-TRPV4^{-/-} cells. (e) Representative images of MYF cells treated with control or TRPV4 siRNA spread on digestible gelatin tagged with Alexa Fluor 647. Invadosomes were observed through phalloidin-Alexa Fluor 488 staining. Quantification of the average degradation area per cell confirmed that TRPV4 silencing induced a specific decrease in invadosome-mediated gelatin degradation (SEM; $n = 3$; >70 cells per condition; unpaired t test), which was associated with a decrease in MMP14 surface expression of treated MYF cells (SEM; $n = 3$; >30 cells per condition; unpaired t test). (f) Representative images of MYF-TRPV4^{-/-} cells that express or not

tgRFP-TRPV4^{WT} spread on digestable gelatin tagged with Alexa Fluor 647. Invadosomes were observed through phalloidin–Alexa Fluor 488 staining. Quantification of the average degradation area per cell confirmed that TgRFP-TRPV4^{WT} expression induced a specific increase in invadosome-induced gelatin degradation (SEM; $n = 3$; >70 cells per condition; unpaired *t* test), which was associated with an increase in MMP14 surface expression in treated MYF cells (SEM; $n = 3$; >30 cells per condition; unpaired *t* test). *, $P \leq 0.05$; **, $P \leq 0.01$; ***, $P \leq 0.001$; ****, $P \leq 0.0001$. Scale bars: 5 μm (a and b), 15 μm (c and d), and 10 μm (e and f).

silencing in MYF cells clearly reduced their efficiency in digesting fluorescently labeled ECM (Fig. 1 e). This effect was supported by a decrease in the surface expression of endogenous MT1-MMP following TRPV4 silencing (Fig. 1 e, right). Moreover, reexpression of tgRFP-TRPV4^{WT} drastically increased both the efficiency of ECM degradation by invadosomes and the surface expression of MT1-MMP in MYF-TRPV4^{-/-} invadosomes, confirming TRPV4 function in the coupling of acto-adhesion and ECM degradation activities (Fig. 1 f). Silencing of TRPV4 in the mouse macrophage cell line RAW264.7 induced an increase in cells forming a high number of podosomes and a general decrease in their degradative activity (Fig. S3). Thus, the function of TRPV4 in regulating ADC appears to be general rather than limited to the MYF cell model.

By positively regulating ECM degradation and negatively regulating acto-adhesion, the plasma membrane Ca²⁺ channel TRPV4 is a new and important regulator of ADC.

TRPV4 regulates the acto-adhesive functions of invadosomes by modulating β 1-integrin activation

The dynamic modulation of β 1-integrin activity is essential for invadosome-induced ECM digestion (Destaing et al., 2010). Since TRPV4 can regulate invadosome size, dynamics, and ADC, we investigated whether TRPV4 regulates the activation of β 1-integrin since both colocalize at the periphery of the invadosome (Fig. 2 a). Thus, the correlation between transient TRPV4 activation and level of active β 1-integrin at the plasma membrane was investigated. TRPV4 activation after 15 min of treatment with the specific TRPV4 activator GSK1016790A (100 nM) led to a significant decrease in the surface expression of β 1-integrin in its active conformation (revealed by 9EG7 antibody) without affecting the total amount of β 1-integrin at the cell surface (revealed by MBI-2 antibody staining; Fig. 2 b). Considering that active TRPV4 is correlated with decreased β 1-integrin activation, we hypothesized that the loss of TRPV4 was associated with the activation of β 1-integrin. Consistent with the results of TRPV4 activation experiments, TRPV4 silencing resulted in a significant increase in the level of active β 1-integrin at the cell surface (Fig. 2 c).

Therefore, activation of TRPV4 can regulate β 1-integrin activation, which is essential for invadosome functions. This led us to determine the molecular mechanism by which TRPV4 regulates ADC and invadosomes.

Intact and functional TRPV4 is required for proper invadosome assembly and ADC

Not only is TRPV4 a simple Ca²⁺-selective pore controlling the local entry of Ca²⁺, but it also is characterized by the presence of numerous intracellular interaction domains, such as the proline-rich domain (PRD; Garcia-Elias et al., 2008), a domain that interacts with PI(4,5)P2 (PH-like domain; Garcia-Elias et al., 2013), ankyrin domains, and a calmodulin-binding domain (Garcia-

Elias et al., 2008) proximal to a gain-of-function E797K mutation that induces a human TRPV4-dependent channelopathy (Loukin et al., 2015). A reverse genetic approach was used to restore the stable expression of four characterized TRPV4 mutants, and the importance of Ca²⁺ release and the adaptor functions of these channels in invadosomes were tested separately (Fig. 3 a). To test the importance of Ca²⁺ entry downstream of TRPV4 in invadosomes, the pore mutant tgRFP-TRPV4^{M680D} (loss of Ca²⁺ permeation) and the gain-of-function mutant tgRFP-TRPV4^{E797K} (constitutive Ca²⁺ permeation) were expressed in MYF-TRPV4^{-/-} cells. All mutants tagged with tgRFP were stably expressed in MYF-TRPV4^{-/-} cells that were subsequently sorted by FACS in order to have the same tgRFP fluorescence intensity as that observed in the MYF-TRPV4^{-/-}+tgRFP-TRPV4^{WT} cells. MYF-TRPV4^{-/-}+tgRFP-TRPV4^{M680D} cells formed the same number of invadosome rings as MYF-TRPV4^{-/-}+tgRFP-TRPV4^{WT} cells, but their digestion of the ECM was inefficient (Fig. 3, b–d). The inability of TRPV4 to permeate Ca²⁺ therefore strongly perturbs efficient ECM degradation. Interestingly, expression of the gain-of-function mutant tgRFP-TRPV4^{E797K} did not rescue either acto-adhesion or ECM degradation functions of MYF-TRPV4^{-/-} cells (Fig. 3, b–d). These results highlight the need for regulated and optimal Ca²⁺ entry through TRPV4 to establish efficient ADC.

However, the difference in phenotypes between MYF-TRPV4^{-/-}+TagRFP-TRPV4^{M680D} and MYF-TRPV4^{-/-} cells suggests additional regulatory activity of this channel on invadosome functions beyond simple Ca²⁺ modulation. Therefore, we hypothesized that TRPV4 acts as a protein adaptor through a specific protein domain. We focused our investigations on the PI(4,5)P2-binding domain and PRD of TRPV4. The PRD of TRPV4 is especially interesting since it is not present within other members of the TRP vanilloid family (Hellmich and Gaudet, 2014; Huynh et al., 2014). Interestingly, expression of tgRFP-TRPV4^{I21AAWAA}, a mutant in which PI(4,5)P2 binding is abolished (Garcia-Elias et al., 2013), dysregulated ADC since tgRFP-TRPV4^{I21AAWAA} expression increased the formation of invadosomes without increasing ECM degradation in MYF-TRPV4^{-/-} cells (Fig. 3, b–d). In contrast, the expression of tgRFP-TRPV4^{ΔPRD} rescued invadosome formation but did not improve ECM degradation in MYF-TRPV4^{-/-} cells (Fig. 3, b–d). Thus, the PRD seems more important for regulating ECM degradation than the acto-adhesive activity of invadosomes. The impact of each mutation of tgRFP-TRPV4^{WT} on invadosome number was also associated with changes in invadosome perimeter (Fig. S4 a). Interestingly, while tgRFP-TRPV4^{I21AAWAA} showed the same localization at the periphery of the invadosome as tgRFP-TRPV4^{WT}, tgRFP-TRPV4^{ΔPRD} was poorly localized at invadosome rings, showing the essential role of the PRD in targeting of TRPV4 to invadosomes (Fig. S4 b). Contrary to all tested mutants, only reexpression of tgRFP-TRPV4^{WT} can both negatively regulate the surface expression of active β 1-integrin in MYF-TRPV4^{-/-} cells (revealed by FACS analysis of large cell populations; Fig. S4 c) and

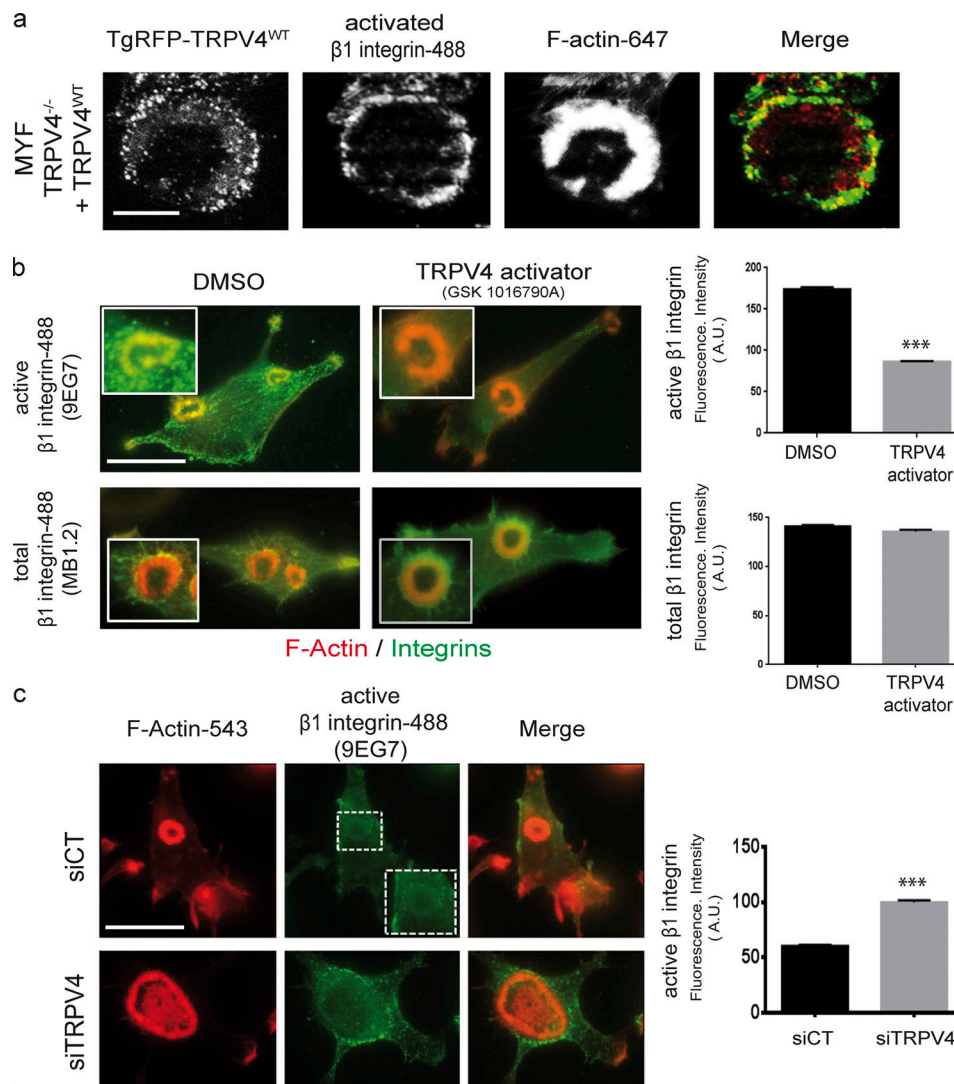


Figure 2. TRPV4 is accumulated with β 1-integrin and regulates its activation in invadosomes. (a) Representative TIRF images of MYF-TRPV4^{-/-} cells stably expressing TgRFP-TRPV4^{WT} stained for active β 1-integrin (9EG7–Alexa Fluor 488) and F-actin (phalloidin–Alexa Fluor 647). (b) Representative images of MYF cells treated with DMSO or the specific TRPV4 activator GSK1016790A (100 nM) for 15 min, then stained for either active β 1-integrin (Ab 9EG7) or total β 1-integrins (Ab MB1-2) and F-actin (phalloidin–Alexa Fluor 543). Quantification of the average intensity of surface expression per cell confirmed that TRPV4 activation specifically decreased the activation of β 1-integrins (SEM; $n = 3$; >40 cells per condition; unpaired t test). (c) Representative images of MYF cells treated with control or TRPV4 siRNA stained for active β 1-integrin (9EG7–Alexa Fluor 488) and F-actin (phalloidin–Alexa Fluor 543). Quantification of the average intensity of surface expression per cell confirmed that TRPV4 silencing specifically increased active β 1-integrin staining (SEM; $n = 3$; >40 cells per condition; unpaired t test). *, $P \leq 0.05$; **, $P \leq 0.01$; ***, $P \leq 0.001$; ****, $P \leq 0.0001$. Scale bars: 7 μ m (a) and 15 μ m (b and c).

decrease rapid spreading on the β 1-integrin-associated substrate fibronectin (Fig. S4 d). Thus, these rescued experiments confirm that both adaptor and calcium-pore functions of TRPV4 have complex and important roles in the dynamic regulation of β 1-integrin activation.

A structure–function study highlighted the necessity of coupling Ca²⁺ permeation and PI(4,5)P₂- or PRD-associated protein complex formation to support full TRPV4 activity in efficiently regulating invadosomes.

Identification of specific interactors of TRPV4 in invadosomes reveals new ADC regulatory pathways downstream of TRPV4

The importance of the coupling between Ca²⁺ permeation and TRPV4 adaptor functions led us to characterize protein complexes associated with TRPV4 in the specific environment of the

invadosome. Rescued expression of tgRFP-TRPV4^{WT} and tgRFP-TRPV4 mutants in MYF-TRPV4^{-/-} cells was used for coimmunoprecipitation (coIP) of both tgRFP-TRPV4 and their associated proteins (Fig. 4 a). Since Ca²⁺ permeation can affect binding of TRPV4 partners, we decided to pool label-free semi-quantitative mass spectrometry analyses of the coIP of tgRFP-TRPV4^{WT} with the nonpermissive tgRFP-TRPV4^{M680D} mutant and the constitutively active tgRFP-TRPV4^{E797K} mutant (Data S1). Several known TRPV4 interactors, such as CTPS1, SRC, DDX1, and AUF1, were sorted out, validating our approach. Several sorted proteins were found to be involved in vesicular trafficking (e.g., SEC13 and MYO1C) and stress granule formation (DDX1); interestingly, most of the proteins (>70%) were involved in redox signaling as they were ROS-related or ROS-sensitive proteins

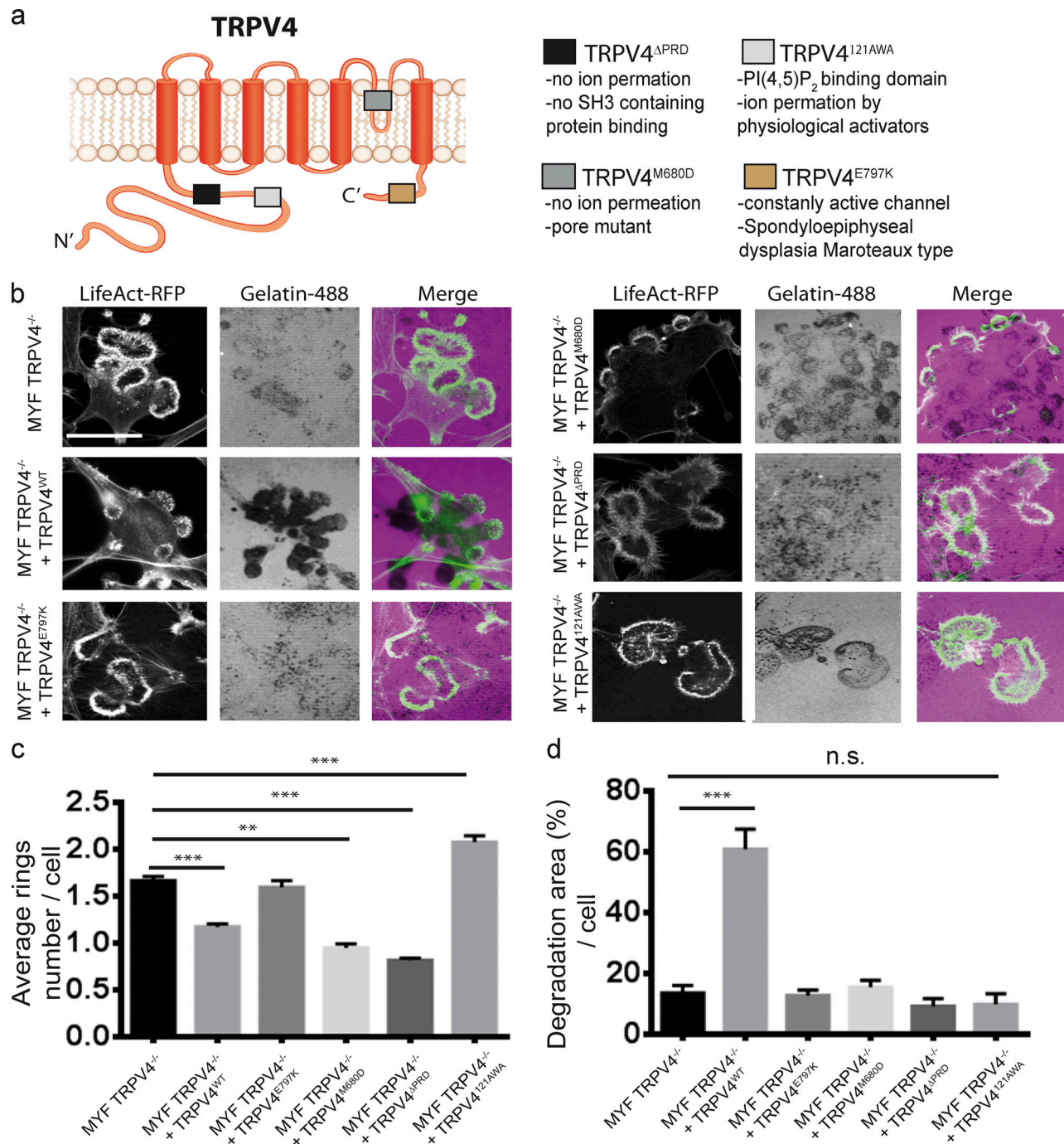


Figure 3. Synergy between calcium permeation and adaptor activities of TRPV4 sustains ADC in invadosomes. (a) Schematic of TRPV4 organization in the plasma membrane. The different mutations used are indicated, and the results of their investigation are detailed. (b) Representative images of MYF-TRPV4^{-/-} cells stably expressing TgRFP-TRPV4^{WT} or the indicated TgRFP-TRPV4 mutant spread on digestible gelatin–Alexa Fluor 488. Invadosomes were observed through phalloidin–Alexa Fluor 647 staining. (c) Quantification of the average number of invadosome rings per MYF-TRPV4^{-/-} cell stably expressing TgRFP-TRPV4^{WT} or the indicated TgRFP-TRPV4 mutant (SEM; n = 3; >150 cells per condition; unpaired t test). (d) Quantification of the average degradation area per cell in MYF-TRPV4^{-/-} cells stably expressing TgRFP-TRPV4^{WT} or the indicated TgRFP-TRPV4 mutant (SEM; n = 3; >150 cells per condition; unpaired t test). The expression of only TgRFP-TRPV4^{WT} induced the formation of efficient invadosomes able to digest ECM. *, P ≤ 0.05; **, P ≤ 0.01; ***, P ≤ 0.001; ****, P ≤ 0.0001. Scale bar: 15 μm (b). n.s., not significant.

(such as the mitogen-activated kinases ASK1 and ASK2; Fig. 4 a). As expected, our approach also revealed several Ca²⁺-related proteins (such as unconventional MYO1C and ASK1). To confirm the validity of our coIP approach, Flag-ASK1 and tgrFP-

TRPV4^{WT} constructs were cotransfected into HEK293 cells that were subjected to immunoprecipitation assays. Both proteins were coimmunoprecipitated with an antibody against tgrFP, confirming the interaction between TRPV4 and ASK1 (Fig. 4 b).

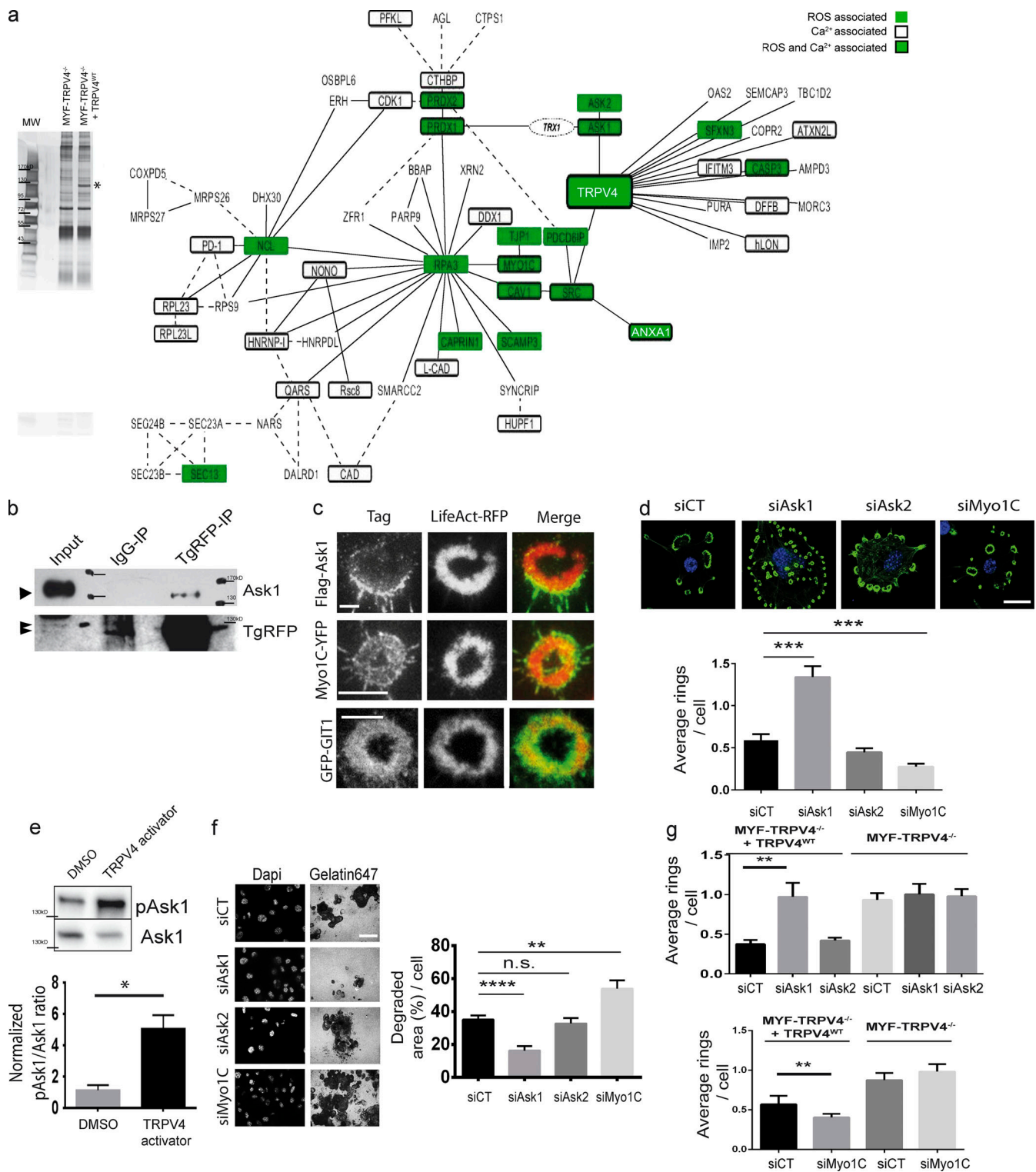


Figure 4. The TRPV4-binding partners ASK1 and MYO1C regulate ADC in invadosomes. (a) Silver staining analysis of TRPV4 partners copurified with TgRFP-TRPV4^{WT} expressed in MYF-TRPV4^{-/-} cells using anti-TgRFP antibody (# corresponds to the TgRFP-TRPV4^{WT} band). Direct protein-protein interaction network was used to show that the majority of these potential TRPV4 partners were known to interact between each other in a public database. Proteins not known to interact between each other in the database were left on the right side of the network and directly connected to TRPV4. GO and literature analysis highlighted proteins exhibiting an association with ROS signaling (green), Ca²⁺ signaling (dark frame), or both (green and dark frame). (b) The specific coIP of ASK1-Flag and TgRFP-TRPV4^{WT} overexpressed in HEK293 cells shows the specific interaction between these two proteins, which confirmed the mass spectrometry data. (c) Representative images of MYF cells stably expressing LifeAct-RFP transfected with the indicated potential TRPV4 partners identified by mass spectrometry. As ASK1 binds TgRFP-TRPV4^{WT}, only MYO1C-YFP accumulates at the invadosome periphery, in contrast with the control GFP-GIT1. (d) Representative images of MYF cells treated with control or the indicated siRNAs and stained with phalloidin-Alexa Fluor 488 and DAPI. ASK1 silencing

induced a strong increase in invadosome formation, while MYO1C depletion decreased invadosome ring formation (SEM; $n = 3$; >150 cells per condition; unpaired t test). **(e)** Treatment of HEK cells transfected with ASK1-Flag and tgRFP-TRPV4^{WT} with DMSO or the specific TRPV4 activator GSK1016790A (100 nM) for 15 min induced the specific activation of ASK1 (measured in Western blot by the P-T845ASK1/total ASK1 ratio; SEM; $n = 3$; unpaired t test). **(f)** Representative images of MYF cells treated with control or the indicated siRNAs spread on digestible gelatin–Alexa Fluor 647. The cell number was determined through DAPI staining. Quantification of the average degradation area per cell upon treatment with different siRNAs confirmed that ASK1 silencing strongly decreased ECM degradation, while MYO1C depletion increased the efficiency of invadosome-induced degradation (SEM; $n = 3$; >100 cells per condition; unpaired t test). Thus, the TRPV4-associated proteins ASK1 and MYO1C antagonistically regulate ADC. **(g)** Quantification of the average number of invadosomes per cell in MYF-TRPV4^{-/-} cells that were or were not rescued with TgRFP-TRPV4^{WT} treated with the indicated siRNA. The ability of ASK1 and MYO1C to increase invadosome formation is downstream of TRPV4 activity (SEM; $n = 3$; >150 cells per condition; unpaired t test). *, $P \leq 0.05$; **, $P \leq 0.01$; ***, $P \leq 0.001$; ****, $P \leq 0.0001$. Scale bar: 8 μm (c), 15 μm (d), and 20 μm (f). n.s., not significant.

To confirm it, we coimmunoprecipitated ASK1 and tgRFP-TRPV4^{WT} (or the indicated mutant) and showed that tgRFP-TRPV4 ^{Δ PRD}, tgRFP-TRPV4^{E797K}, and tgRFP-TRPV4^{I21AWA} were still binding ASK1. Thus, the PRD domain of TRPV4 is not fully mediating the interaction with ASK1 (Fig. S5 a).

To easily confirm the relevance of numerous other potential TRPV4 partners at the invadosome, we determined the localization of these TRPV4 partners in the invadosome ring and compared the results with the characteristic localization of TRPV4 at the invadosome periphery. ASK1 and unconventional MYO1C were specifically localized at the invadosome periphery in contrast to the control GFP-GIT1 (Fig. 4 c). Specific staining of endogenous MYO1C confirmed its accumulation at the invadosome periphery (Fig. S5 b) and confirmed that reexpression of each TRPV4 mutant used in MYF-TRPV4^{-/-} cells did not drastically perturb this specific localization (Fig. S5 c). The specific localization of ASK1 and MYO1C highlighted their possible functional link with TRPV4.

To test the functional relevance of ASK1 and MYO1C downstream of TRPV4, we investigated whether these proteins could also regulate ADC as TRPV4, indicated by an increase in the number of invadosomes that poorly degrade ECM. Invadosome formation and ECM degradation were quantified following ASK1 and MYO1C silencing. The siRNA efficiency was confirmed by quantitative PCR (qPCR; Fig. S5 d). Interestingly, ASK1 silencing in MYF cells reduced ADC since it dramatically increased the formation of invadosome rings (Fig. 4 d) and significantly decreased ECM degradation (Fig. 4 f), which mimicked the effects of TRPV4 KO. In addition, overexpression of ASK1-WT kinase and the kinase-dead ASK1^{R256C} mutant confirmed the essential role of ASK1 kinase activity in invadosome morphology (Fig. S5 e). Finally, the essential regulatory role of ASK1 on ADC seems specific since the effects of ASK2 silencing were minor. Interestingly, MYO1C silencing increased ADC since it decreased invadosome formation and increased ECM degradation (Fig. 4, d and f). To confirm the importance of the negative effect of MYO1C on ADC, we used a pharmacological approach to specifically inhibit MYO1C ATPase activity with pentachloropseudilin (PCIP) at 100 μM (Martin et al., 2009; Chung et al., 2018). 14 h of PCIP treatment induced a strong increase in the degradative activity of MYF cells, which mimicked MYO1C silencing (Fig. 4 f and Fig. S5 g). ADC induced by ASK1 or MYO1C silencing highlights the important dynamic range of potential ADC responses.

Considering that ASK1 silencing phenocopied TRPV4 loss of function in invadosomes and that ASK1 requires Ca²⁺ to function, we determined whether Ca²⁺ entry through TRPV4 regulates ASK1 activation. To this end, both tgRFP-TRPV4 and Flag-ASK1

were expressed in HEK293 cells, which were treated with the TRPV4 activator GSK1016790A, following monitoring of ASK1 phosphorylation (Thr845, ASK1 active state) by Western blotting. 10 min of incubation with the TRPV4 activator was sufficient to activate ASK1, as indicated by an increase in the phospho (p)ASK1/ASK1 ratio (Fig. 4 e and Fig. S5 f). Since TRPV4 is able to activate ASK1, we tested whether ASK1 is functionally downstream of TRPV4. ASK1 silencing affected invadosome ring formation only when tgRFP-TRPV4 was expressed in MYF-TRPV4^{-/-} cells, indicating that ASK1 is functionally downstream of TRPV4 (Fig. 4 g). Interestingly, MYO1C silencing also affected invadosome ring formation (Fig. 4 g) and its degradative activity (Fig. S5 h) only when tgRFP-TRPV4 was expressed in MYF-TRPV4^{-/-} cells. All these data support the role of ASK1 and MYO1C as important downstream elements of the TRPV4-dependent signaling pathway implicated in the regulation of ADC in invadosomes.

The identification of TRPV4 partners in invadosome-forming cells reveals a novel TRPV4–ASK1–MYO1C functional complex that dynamically regulates the coupling of acto-adhesion and ECM degradation in invadosomes.

TRPV4 senses ROS that are essential to regulate ADC in invadosomes

The dynamic regulation of ADC raised the question of which stimuli can modulate the functions of the TRPV4-associated complex. Since we identified many ROS-sensitive proteins in our analysis of the TRPV4-associated complex (Fig. 4 a), such as ASK1 (a mitogen-activated protein kinase [MAPK] activated by ROS; Hattori et al., 2009; Nishida et al., 2017), we decided to revisit ROS functions in invadosome biology and ADC in particular. Indeed, ROS signaling was reported to be essential for invadosome function since the general antioxidant N-acetyl cysteine inhibited both invadosome formation and ECM degradation (Diaz et al., 2009). Therefore, we hypothesized that locally produced ROS (extra- and/or intracellular) are sensed by TRPV4 to regulate downstream proteins associated with TRPV4, such as ASK1, and thus control the efficiency of ADC.

To investigate the potential activity of ROS in ADC, MYF cells were first treated with increasing doses of the cell-permeable oxidant H₂O₂ (from 10 μM to 1,000 μM). Surprisingly, increasing H₂O₂ treatment led to a transient increase in the formation of invadosome rings (which peaked at 100 μM H₂O₂ treatment) associated with a constitutive decrease in ECM degradation (Fig. 5, a and b; and Fig. S6 a). Treatment with high concentrations of H₂O₂ inhibited both invadosome formation and ECM degradation. Thus, ROS induction mimicked by H₂O₂

treatment regulates ADC in a biphasic dose-dependent manner and shows the importance of optimal ROS signaling in ADC rather than the simple binary dependence of invadosomes on ROS.

To discern the role of intra- versus extracellular ROS activities in ADC, MYF cells were treated with an impermeable cysteine oxidant (5,5'-dithiobis(2-nitrobenzoic acid) [DTNB]). Mimicking extracellular ROS with 4 μ M DTNB treatment also perturbed ADC since DTNB treatment induced an increase in invadosome ring formation and a decrease in ECM degradation (Fig. 5 c). These data clearly support the ability of extracellular ROS to regulate ADC.

To further evaluate the role of ROS in the dynamics and function of invadosomes, we visualized ROS locally at the invadosome. To that end, we fused the genetically encoded redox ratiometric H_2O_2 biosensor Hyper3 (Bilan et al., 2013) with the adhesive protein paxillin, which is localized in invadosomes (Petropoulos et al., 2016). Ratiometric total internal reflection fluorescence (TIRF) imaging at 488 nm/405 nm and 561 nm allowed us to simultaneously follow the dynamics of the invadosome (LifeAct-monomeric RFP) and the local production of ROS in the vicinity of paxillin-Hyper3 in MYF cells. Live imaging showed an increased ROS signal at the peripheries of forming invadosomes (Fig. 5 d). Interestingly, subsequent treatment with the activator GSK1016790A strongly decreased the increase in ROS signal following H_2O_2 treatment in the vicinity of paxillin-Hyper3 in invadosomes (Fig. S6 b).

To confirm that TRPV4 can sense and regulate the ROS signaling implicated in ADC, we first applied increasing doses of H_2O_2 to MYF cells in which TRPV4 expression was silenced. The loss of TRPV4 abolished the biphasic dose-dependent response of invadosome formation to H_2O_2 treatment (Fig. 5 e). In addition, we applied increasing doses of H_2O_2 to MYF-TRPV4^{-/-} cells that did or did not express tgRFP-TRPV4^{WT}, the pore mutant tgRFP-TRPV4^{M680D} (no Ca²⁺ permeation), and the disease-inducing mutant tgRFP-TRPV4^{E797K} (constitutive Ca²⁺ permeation). Expression of tgRFP-TRPV4^{WT} rescued the biphasic dose-dependent response of invadosome formation in MYF-TRPV4^{-/-} cells to H_2O_2 treatment. Consistently, the tgRFP-TRPV4^{M680D} pore mutant failed to rescue the response of MYF-TRPV4^{-/-} cells, confirming the essential role of Ca²⁺ permeation in the ROS signaling pathway controlled by TRPV4. In contrast, expression of the gain-of-function disease-inducing mutant tgRFP-TRPV4^{E797K} rescued the activity of the biphasic dose-dependent response of invadosome formation in MYF-TRPV4^{-/-} cells to H_2O_2 treatment (Fig. 5 f). Interestingly, mimicking extracellular ROS production with DTNB did not affect ring formation in MYF-TRPV4^{-/-}+tgRFP-TRPV4^{E797K} cells (Fig. S6 c). The discrepancy between DTNB and H_2O_2 responses in the presence of the tgRFP-TRPV4^{E797K} mutant suggests that ROS regulatory activity of TRPV4 is different in the presence of extra- and intracellular ROS. Therefore, TRPV4 is an important sensor in the ROS signaling pathway that controls invadosome formation and ADC. This led us to determine the molecular basis of this potential bidirectional ROS-sensing function of TRPV4 in invadosome regulation.

Identification of cysteine residues that support ROS sensing by TRPV4 in ADC

Our data suggest that TRPV4 senses and regulates ROS signaling in invadosomes. We aimed to determine whether ROS can regulate TRPV4 activity in MYF cells. To measure Ca²⁺ entry at the

vicinity of TRPV4, we fused TRPV4^{WT} with the genetically encoded calcium indicator Gcamp-GFP (Nakai et al., 2001) and expressed the fusion protein in MYF-TRPV4^{-/-} cells. H_2O_2 treatment clearly increased the fluorescent signal in MYF-TRPV4^{-/-}-Gcamp-TRPV4^{WT} cells, specifically the signal around invadosome rings (Fig. 6 a and Fig. S7 a).

Cysteines are susceptible to ROS-dependent oxidation, leading to disulfide bridges, and play an important role in the folding and activity of proteins, including ion channels (Tang et al., 2004). To determine the molecular basis of the ROS-sensing activity of TRPV4, we focused on cysteine residues in both the extracellular and the intracellular loops of TRPV4 that share high homology with cysteine residues of the ROS-sensitive TRPV1 channel. Moreover, our interest in identifying important regulatory cysteines was reinforced since several mutations that cause human channelopathies involve the addition of extra- and intracellular cysteines (e.g., R232C, R269C, R316C, Y602C, and R232C; Fig. 6 b; Nilius and Voets, 2013). Therefore, we hypothesized that these mutations increase the formation of additional disulfide bridges with proximal cysteines in the presence of ROS, which then affects TRPV4 structure and activity. Thus, perturbation of the ROS sensitivity of TRPV4 could be an essential mechanism shared by both channelopathies and ADC in invadosomes. First, we targeted extracellular cysteines that share high homology with cysteine residues of the ROS-sensitive TRPV1 channel (Ogawa et al., 2016) and mutated them to alanines (Gcamp-TRPV4^{eCyst} containing C639A, C645A, C652A, and C660A mutations). In addition, we mutated several intracellular cysteines (Gcamp-TRPV4^{iCyst} containing C294A, C353A, and C427A mutations) based on their proximity to arginine 269, since its mutation to a cysteine (R269C; Fig. 6 b) induces Charcot-Marie-Tooth (CMT) disease. These TRPV4 mutants are functional in terms of ion permeation since the TRPV4-Gcamp-GFP signal increased in the same range in response to the TRPV4 activator GSK (Fig. S6 a). Expression of both Gcamp-TRPV4^{eCyst} and Gcamp-TRPV4^{iCyst} in MYF-TRPV4^{-/-} cells increased the formation and size of invadosome rings without increasing their ECM degradative activity (Fig. 6, c and d; and Fig. S7 b). Thus, the simple perturbation of several extra- or intracellular cysteines is sufficient to abolish the regulatory role of TRPV4 in ADC. Interestingly, the significant differential effect of Gcamp-TRPV4^{eCyst} and Gcamp-TRPV4^{iCyst} on invadosome functions confirmed that the regulation of ROS by TRPV4 activity is different in the presence of extra- and intracellular ROS (Fig. 6, c and d).

The importance of TRPV4 cysteines on invadosome regulation led us to determine whether the pathological Gcamp-TRPV4^{R269C} mutant, which induces CMT disease in humans, can regulate ADC. Surprisingly, the expression of Gcamp-TRPV4^{R269C} in MYF-TRPV4^{-/-} cells strongly increased ADC since it reduced invadosome ring formation (Fig. 6, c and d; and Fig. S7 b) and was highly efficient in degrading the ECM (Fig. 6 d). We used this disease-associated TRPV4 mutant to test the importance of the cysteine environment in ADC regulation by TRPV4. The R269C mutation was introduced in Gcamp-TRPV4^{iCyst} (Fig. 6 b). Interestingly, mutation of the cysteines surrounding the R269C mutant into alanines completely rescued changes in the formation of invadosome rings and restored normal ECM degradative activity (Fig. 6, c and d). Thus,

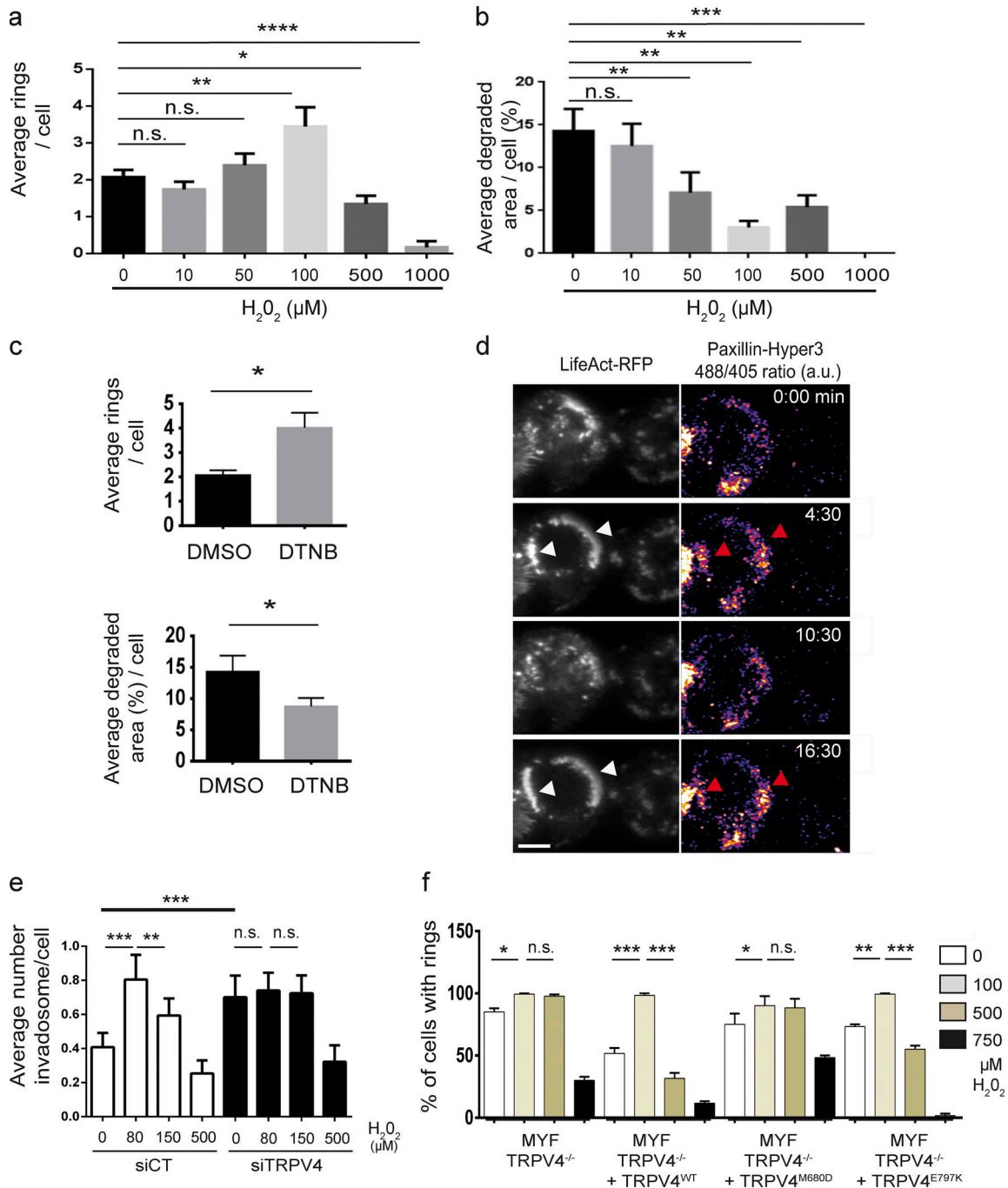


Figure 5. ROS negatively regulate ADC through TRPV4 activity. (a) Quantification of the average number of invadosome rings per cell in MYF cells treated with increasing doses of H₂O₂, which induced a transient increase in invadosome ring formation (SEM; *n* = 3; >150 cells per condition; unpaired *t* test). (b) Quantification of the average degradation area per MYF cell upon treatment with increasing doses of H₂O₂ showed that increased ROS concentration reduced constitutive invadosome-induced ECM degradation (SEM; *n* = 3; >70 cells per condition; unpaired *t* test). Since they uncouple invadosome formation and ECM degradation, ROS are newly identified negative regulators of ADC. (c) Quantification of the average number of invadosomes (SEM; *n* = 3; >150 cells per condition; unpaired *t* test) and degradation area (SEM; *n* = 3; >70 cells per condition; unpaired *t* test) per MYF cell treated with the extracellular oxidant DTNB. Mimicking extracellular ROS activity also negatively regulated ADC by increasing invadosome formation and decreasing invadosome-induced degradation. (d) Representative images of MYF cells expressing both LifeAct-RFP and paxillin-Hyper3 to observe the dynamics of intracellular ROS (visualized by the 488 nm/405 nm ratio) in the vicinity of invadosomes. The formation of invadosome rings (white arrowheads) is associated with an increase in the 488 nm/405 nm ratio (red arrowheads). (e) Quantification of the average number of invadosomes per cell in MYF cells treated with control and TRPV4 siRNAs with increasing doses of H₂O₂ (SEM; *n* = 3; >150 cells per condition; unpaired *t* test). TRPV4 silencing abolished sensitivity to ROS in the regulation of invadosome formation. (f) Quantification of the average number of invadosomes per cell in MYF-TRPV4^{-/-} cells that were or were not rescued with TgRFP-TRPV4^{WT}, the permeation mutant TgRFP-TRPV4^{M680D}, and the disease-associated mutant TgRFP-TRPV4^{E797K} treated with increasing doses of H₂O₂ (SEM; *n* = 3; >150 cells

per condition; unpaired *t* test). These results show the importance of calcium permeation regulation through TRPV4 in the regulation of ROS-dependent invadosome formation. *, $P \leq 0.05$; **, $P \leq 0.01$; ***, $P \leq 0.001$; ****, $P \leq 0.0001$. Scale bar: 5 μm (d). n.s., not significant.

reducing the possibility of forming disulfide bridges around the R269C mutant abolished the biological ADC activity of this pathological mutant.

The impact of the mutations that were sufficient to modulate ADC without affecting calcium permeation (Fig. 6 a) led us to determine whether the ROS sensitivity of TRPV4 is supported in these mutants. Thus, MYF-TRPV4^{-/-} cells expressing Gcamp-TRPV4^{eCyst} and Gcamp-TRPV4^{iCyst} mutants were treated with increasing doses of H₂O₂ or the extracellular cysteine-specific oxidant DTNB. The biphasic dose-dependent response following H₂O₂ treatment was perturbed in MYF-TRPV4^{-/-} cells expressing the Gcamp-TRPV4^{eCyst} or Gcamp-TRPV4^{iCyst} mutants. This result clearly shows that both groups of cysteines are directly involved in ROS sensing. In addition, the effects of DTNB treatment on invadosome formation were reduced in the presence of the Gcamp-TRPV4^{eCyst} and Gcamp-TRPV4^{iCyst} mutants (Fig. 6 c). This result suggests that TRPV4 is more sensitive to intracellular ROS signaling than extracellular ROS signaling.

The mutated cysteines appear to be the core of TRPV4 ROS sensitivity. Both intra- and extracellular ROS sensitivity affected ADC to the same extent. This result confirmed the participation of TRPV4 in bidirectional ROS signaling. Finally, the link between specific TRPV4 mutations leading to CMT channelopathy and ROS signaling suggests a novel general molecular mechanism essential in TRPV4 functions and therapeutic approaches.

Discussion

Investigating the role of the calcium permeation and adaptor functions of the TRPV4 channel in invadosome biology showed its essential role in controlling the coupling between actin-adhesion and ECM degradation (ADC; Fig. 7). Identification of its partners revealed the essential activity of TRPV4 in sensing and regulating the newly described functions of ROS in ADC.

Essential role of TRPV4 in mechanotransduction

Our data emphasize the functions of TRPV4 at invadosomes. Among all TRP family proteins, only TRPV2 has been shown to be associated with podosomes (Nagasawa and Kojima, 2012). Thus, TRPV4 appears now as a ubiquitous regulator of most adhesive structures. The functions of TRPV4 in invadosome confirmed its generic role in the mechanotransduction processes associated with cell migration of multiple cell types (Alessandri-Haber et al., 2008). In the mechanoreponse of osteoblastic cells, a recent report even suggested that TRPV4 could be more important than the calcium channel Piezo1, thought to be the main channel implicated in mechanotransduction (Yoneda et al., 2019).

The mechanotransduction function of TRPV4 is mainly associated with factors downstream of β 1-integrin (Schiller and Fässler, 2013; Milloud et al., 2017). Indeed, the application of force on β 1-integrin induced mechanosensitive calcium influx through TRPV4 channel activation and relocalization at the plasma membrane (Matthews et al., 2010). Thus, the perturbation of

TRPV4 activity or expression affects cell shape, adhesion, and spreading, alters cell contractility, and decreases directional migration (Thodeti et al., 2009; Mrkonjić et al., 2015). The activity of TRPV4 appears essential even in regulating the assembly of collagen fibers, the main ECM target of β 1-integrins, through regulating mechanical forces (Gilchrist et al., 2019). Interestingly, TRPV4 activity at invadosomes appeared essential to negatively regulate β 1-integrin activation (Fig. 2; and Fig. S4, c and d). Thus, the importance of TRPV4 in invadosomes explains molecularly why β 1-integrin should not be constitutively active but should oscillate between active and inactive states to sustain efficient ADC (Destaing et al., 2010). However, the precise mechanism by which TRPV4-dependent Ca²⁺ entry negatively regulates β 1-integrins remains unknown. We hypothesize that TRPV4 could be important for regulating calpain activity, which inhibits β 1-integrins through calcium-sensitive cleavage of the β 1-integrin activator talin1 (Franco et al., 2004).

TRPV4 assembles calcium- and ROS-sensitive complexes in adhesive structures

TRPV4 interacts with β 1-integrins and adhesion regulators, such as the tyrosine kinase c-SRC (Alessandri-Haber et al., 2008). Considering the multiple domains implicated in its activity, TRPV4 is associated with regulating calcium release and the recruitment of large protein complexes. The identified TRPV4-binding partners in invadosome-forming cells were not only enriched in invadosome regulators, such as the calcium-dependent AnnexinA1, the mechanosensitive- and ROS-dependent caveolin1, and the ROS- and calcium-dependent c-SRC (Mallawaarachy et al., 2015; Bizzarro et al., 2012; Yang et al., 2016; Yoo et al., 2012) but also included numerous Ca²⁺-sensitive proteins implicated in ROS signaling, such as the ASK kinases.

At steady state, ASK1 is an MAPK that oligomerizes and is maintained in an inactive form by the ROS-sensitive protein thioredoxin and CIB1 (Hattori et al., 2009; Leisner et al., 2016). Like TRPV4, ASKs are activated by osmotic, chemical, thermal, and mechanical cues and ROS (Hattori et al., 2009). With the exception of a voltage-dependent calcium channel, the source of the calcium that activates ASK1 has been poorly investigated (Hattori et al., 2009). Our data suggest that TRPV4 is a new source of Ca²⁺ that activates ASK1 (Fig. 4 e). In cancer, the gene encoding ASK1 harbors a recurrent somatic mutation, ASK1^{R256C} (Prickett et al., 2014), that perturbed invadosome morphology in MYF cells (Fig. S2 b). In addition to containing numerous ROS-sensitive cysteines, TRPV4 is now known to be heavily involved in ROS signaling through its essential downstream partner ASK1.

We also identified the CIB1-binding partner MYO1C as a TRPV4 interactor. MYO1C is a calcium-sensitive short-tailed myosin characterized by its slow ATPase rate. Thus, MYO1C has been implicated in cargo transport and the cross-linking of stress-bearing actin filament barriers close to the plasma membrane (Bond et al., 2013). MYO1C is an essential myosin in

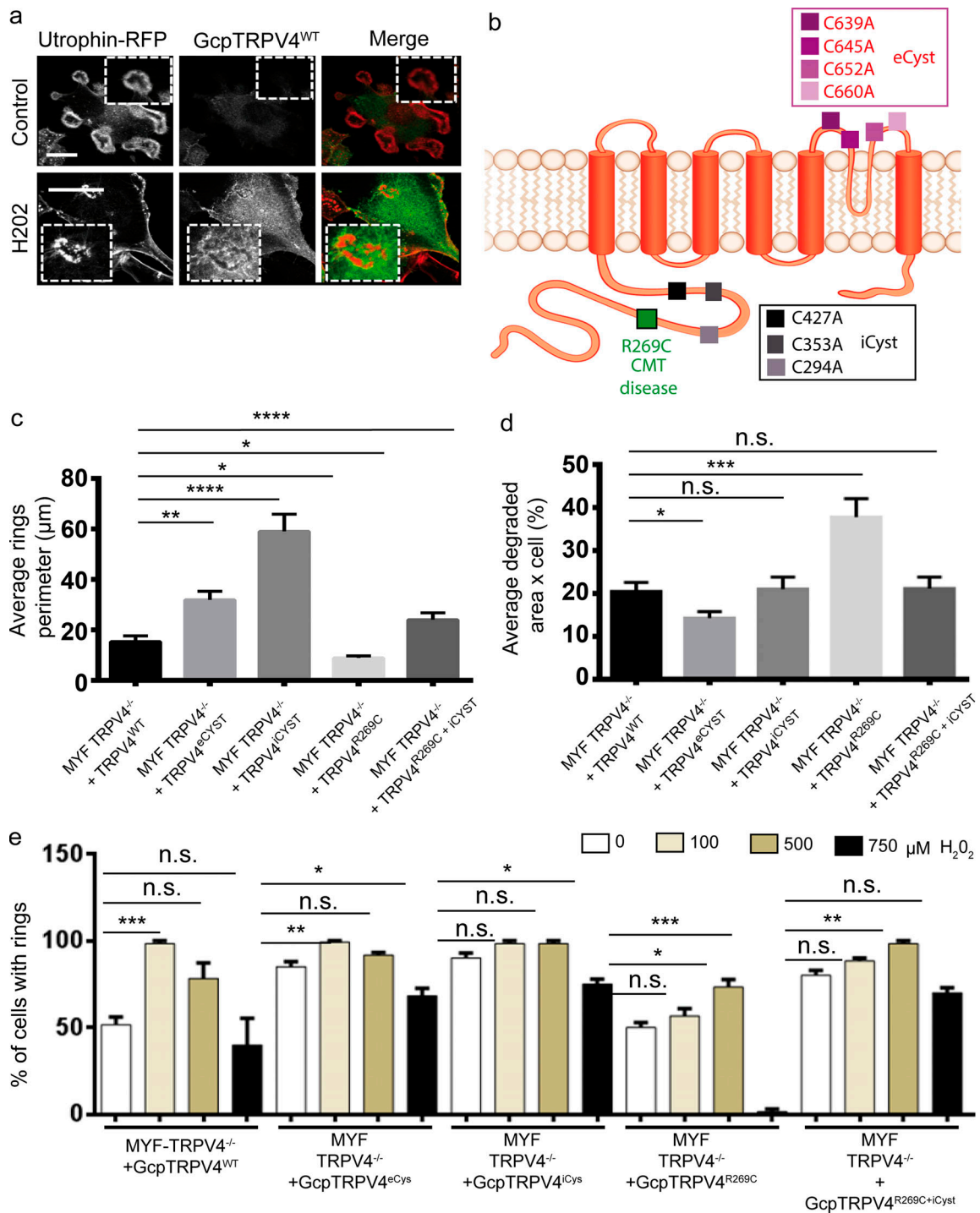


Figure 6. The ROS-sensing function of TRPV4 in ADC is bidirectional and mediated by extra- and intracellular stretches of cysteines that can rescue the activity of pathological cysteine mutations (TRPV4^{R269C}). (a) Representative images of MYF-TRPV4^{-/-} cells stably expressing Gcamp-TRPV4^{WT} treated with 100 μM H₂O₂ for 15 min. Zoom of invadosome rings in white boxes. Increasing ROS concentrations induced calcium permeation in the vicinity of TRPV4 and directly showed its ROS-sensitive activity. (b) Schematic of TRPV4 organization and disposition of the extra- and intracellular cysteines mutated into alanines to avoid the formation of disulfide bridges. Mutated intracellular cysteines were chosen based on their structural proximity to R269, which, when mutated into cysteine, leads to CMT disease and potentially affects ROS sensitivity. (c) Quantification of the average number of invadosomes per cell in MYF-TRPV4^{-/-} cells rescued with Gcamp-TRPV4^{WT} and the indicated Gcamp-TRPV4 mutants affecting disulfide bridge formation. Mutation of both the extra- and intracellular cysteines increased invadosome formation. Mutation of the intracellular stretch of cysteines rescued the ability of the disease-associated Gcamp-TRPV4^{R269C} mutant to decrease invadosome formation (SEM; n = 3; >150 cells per condition; unpaired t test). (d) Quantification of the average degradation area per cell of MYF-TRPV4^{-/-} cells rescued with Gcamp-TRPV4^{WT} and the indicated Gcamp-TRPV4 mutants that affect disulfide bridge formation. Only the mutation of extracellular TRPV4 cysteines decreased ECM degradation and invadosome formation. In addition, the mutation of an intracellular stretch of cysteines rescued the ability of the disease-associated Gcamp-TRPV4^{R269C} mutant to increase invadosome formation (SEM; n = 3; >150 cells per condition; unpaired t test). (e) Quantification of the percentage of cells with rings under increasing H₂O₂ concentrations (0, 100, 500, 750 μM) for MYF-TRPV4^{-/-} cells rescued with Gcamp-TRPV4^{WT} and the indicated Gcamp-TRPV4 mutants. Only the mutation of extracellular TRPV4 cysteines decreased the percentage of cells with rings. In addition, the mutation of an intracellular stretch of cysteines rescued the ability of the disease-associated Gcamp-TRPV4^{R269C} mutant to increase the percentage of cells with rings.

unpaired *t* test). Thus, modulating the potential to form extra- or intracellular disulfide regulates ADC. **(e)** Quantification of the average number of invadosomes per cell in MYF-TRPV4^{-/-} cells rescued with Gcamp-TRPV4^{WT} or the indicated Gcamp-TRPV4 mutants that affect disulfide bridge formation treated with increasing doses of H₂O₂ (SEM; *n* = 3; >150 cells per condition; unpaired *t* test). The mutation of both the extra- and intracellular cysteines abolished the ROS-dependent transient increase in invadosome formation, implicating TRPV4 in bidirectional ROS signaling. *, *P* ≤ 0.05; **, *P* ≤ 0.01; ***, *P* ≤ 0.001; ****, *P* ≤ 0.0001. Scale bar: 7 μm (a). n.s., not significant.

mechanoresponses since its actin-attachment lifetime in an environment that inhibits its working stroke is increased. Moreover, MYO1C is able to enter the nucleus to regulate transcription in response to calcium (Greenberg et al., 2012; Maly and Hofmann, 2016). The negative impact of MYO1C on ADC suggests that it could affect invadosome functions by regulating the endocytosis/exocytosis of key factors such as MMP14 and β1-integrins. The activation of this process could be regulated by the CamKII-ASK1 pathways since CamKII perturbation affects MYO1C trafficking activity (Kashiwase et al., 2005; Yip et al., 2008).

Even though the activity of ASK1 and MYO1C depends on the presence of TRPV4 (Fig. 4 g), the molecular interplay between them is not clear. Our work did not provide evidence that these three proteins form a stable complex, since MYO1C is still able to be localized in invadosomes without TRPV4 (Fig. S5 c). However, the binding of TRPV4 and ASK1 seems constitutive since it was observed for all mutants (Fig. S5 a). Further biochemical and proximity-labeling assays will be needed to quantify these interactions and to determine the precise sequence of biochemical events downstream of ROS-sensing by TRPV4. Identification of both ASK1 and MYO1C downstream of TRPV4

strongly suggests the importance of the protein CIB1 in the regulation of their interactions. Interestingly, silencing of CIB1 also induces perturbation of ADC, as indicated by the regular invadosome formation associated with poor ECM degradative activity (Donnelly et al., 2017). In this functional complex, it is clear that extracellular ROS activation of TRPV4 will lead to ASK1 activation (Fig. 4 e) and thus probably amplify a general intracellular ROS response, the magnitude of which could depend on the integration of both ASK1-phosphorylation activity and TRPV4-dependent calcium release. Identifying new specific substrates of ASK1 in the context of invadosomes such as MYO1C or its partner should deeply improve our understanding of the TRPV4-ASK1-MYO1C pathway.

Functions of ROS in ADC

The characterization of TRPV4 partners in invadosomes led us to reconsider the importance of ROS signaling in ADC. Invadosomes are essential for cancer metastasis (Paterson and Courtneidge, 2018), and ROS have been described as protumor factors in tumor progression (Marengo et al., 2016). During invasion, extracellular ROS sensed by TRPV4 can have many origins since they can be induced by integrins (Taddei et al., 2007; Chiarugi et al., 2003), acidic lysosome exocytosis, or acidization with an Na⁺/H⁺ exchanger associated with nonspecific degradation of the ECM (Stock and Pedersen, 2017). However, the detection of local ROS levels could be very important to determine why invadosomes do not digest ECM at all times. This could explain why the regulation of ADC or digestion on demand is essential for efficient invasion, since these processes favor passage of the nucleus through the pores in 3D collagen networks (Infante et al., 2018). The striking ability of Gcamp-TRPV4^{eCyst} to induce large invadosome rings (Fig. S7 b) reminiscent of the podosome belt/sealing zone in osteoclasts suggests the potential importance of ROS sensing by TRPV4 in bone resorption. This is in line with both functions of TRPV4 and ROS within the cytoplasm and extracellular medium in the regulation of the late stage of osteoclastogenesis and bone degradation (Masuyama et al., 2012; Agidigbi and Kim, 2019).

The relationship between ROS and invadosome functions was first described through characterizing Tks protein functions in invadosomes. Tks proteins and integrin activation favor ROS production through the regulation of Nox proteins (Gianni et al., 2009, 2010). ROS are generated extra- and intracellularly and then support a bidirectional signaling process. Previously, the perturbation of endogenous ROS with a general antioxidant was shown to inhibit ECM degradation (Diaz et al., 2009). By revisiting the effects of ROS on both functions, we were able to show that ROS have a more subtle function, since their optimal concentrations both increase invadosome formation and decrease ECM degradation, thus negatively regulating ADC (Fig. 6).

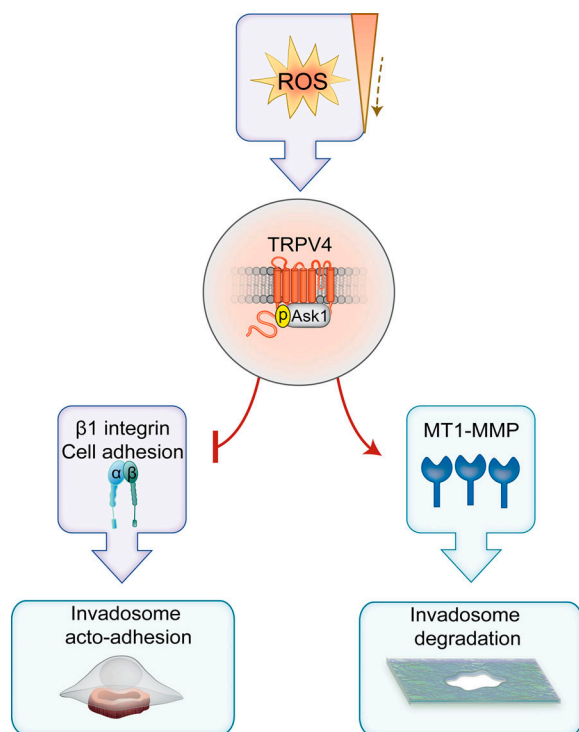


Figure 7. **Schematic of the central role of TRPV4, which regulates both acto-adhesion and ECM degradation in invadosomes, in regulating ADC downstream of ROS sensing.**

These data could explain why the phosphorylation status of Tks4 affects ADC (Buschman et al., 2009). Moreover, the newly described importance of ROS in ADC clearly now supports the importance of HIC-5 (meaning Hydrogen Peroxide-Inducible Clone-5) rather than its homologue paxillin in the activation of matrix degradation in invadosomes (Petropoulos et al., 2016).

The new importance of ROS in regulation of the mechanoregulator TRPV4 raises the question of this specific secondary messenger in mechanotransduction. Even if we cannot provide clear elements to explain this relationship, it is important to consider that activation of the membrane phosphatase RPTP α , another important mechanoregulator in adhesive sites, is also fully dependent on ROS (von Wichert et al., 2003; Groen et al., 2008). Thus, our work highlights the importance of reconsidering the global impact of ROS in mechanotransduction.

ROS induce the formation of disulfide bonds that change protein conformations and activate proteins. Other proteins implicated in ADC are also ROS sensitive. In addition to Tks proteins, the β 1-integrins (de Rezende et al., 2012) and the kinases c-SRC and c-LYN are especially ROS sensitive (Giannoni et al., 2005, 2010; Kemble and Sun, 2009; Yoo et al., 2011).

TRPV4 and ROS in diseases

TRP channels are universal cell sensors of changes in redox status that integrate ROS and calcium signals (Garcia-Elias et al., 2014). However, the relevant context for this sensing function is far from clear. Interestingly, some TRPVs (e.g., TRPV1 and TRPV4) have been associated with ROS signaling (Kozai et al., 2014; Hong et al., 2016). Most TRPs sense ROS through extracellular cysteines in the loop between transmembranes 5 and 6, but the specific roles of each cysteine residue remain unknown. In addition, the use of point mutants and permeable or extracellular ROS treatment clearly indicates that TRPV4 integrates ROS sensing bidirectionally (Fig. 6, Fig. S6, and Fig. S7). In addition, to the best of our knowledge, our data support the role of transient TRPV4 activation in protecting against oxidative stress through ASK activation for the first time.

Characterization of the link between integrins and TRPV4 activity in ROS signaling led us to revisit this link in the context of TRPV4-associated diseases. Indeed, point mutations in the TRPV4 gene cause several human diseases that affect the skeletal and peripheral nervous systems (Nilius and Voets, 2013). Several reports showed that TRPV4 activation can increase ROS in cultured human coronary artery endothelial cells and human coronary arterioles (Bubolz et al., 2011). How mutations in a single gene (here, TRPV4) can cause phenotypically distinct diseases, such as skeletal dysplasias and peripheral neuropathies, remains puzzling and unclear. Based on the data in this report, we suggest that apparently different diseases are linked by the ability of TRPV4 to sense and adjust ROS signaling. ROS production is known to play a role in both the pathophysiology of neurodegenerative diseases and the regulation of bone remodeling (Knowles et al., 2014; Banfi et al., 2008). We provide evidence that both mutants (TRPV4^{E797K} and TRPV4^{R269C}; Fig. 5 and Fig. 6) that cause severe skeletal phenotypes in patients exhibit different sensitivity to ROS (Nilius and Voets, 2013). Therefore, ROS sensitivity and regulation by TRPV4 could be the

missing piece of the puzzle to explain why and how patients with a single TRPV4 point mutation manifest both skeletal and neurodegenerative diseases.

Due to the availability of specific drugs that target the TRPV4 ion channel, this protein is an attractive therapeutic target for TRPV4-associated diseases, cancer metastasis, neurodegenerative diseases, and ASK1-dependent diseases due to the involvement of ADC in these pathologies.

Materials and methods

Antibodies and reagents

Mouse monoclonal antibody against ASK1 (clone H-2) was obtained from Santa Cruz. Rat monoclonal antibody against active β 1-integrin (9EG7) and mouse monoclonal antibody against paxillin (clone 394) were obtained from BD PharMingen. Rat monoclonal antibody against total β 1-integrin (MB1.2) was obtained from EMD Millipore. Rat monoclonal antibody against integrin β 3 (LucA5) was obtained from Emfret. Rabbit monoclonal antibody against MMP14 (EPI264Y) was obtained from Abcam. Rabbit monoclonal antibody against phospho-ASK1 was obtained from Cell Signaling. The different IgG controls were obtained from Abcam. All antibodies are detailed in Data S1. Alexa Fluor 488-, 546-, and 647-labeled phalloidin and Alexa Fluor 488-, 546-, and 647-conjugated secondary antibodies (goat anti-mouse and goat anti-rabbit) were purchased from Invitrogen. Alexa Fluor 647 succinimidyl ester (NHS) was obtained from Life Technologies (#A20006) and was used to color gelatin. TRPV4 channel agonist GSK1016790A was obtained from Sigma-Aldrich (reference G0798), and it was used at 100 nM over 15 min. Hydrogen peroxide solution 30% (wt/wt) was also obtained from Sigma-Aldrich (reference H1009) and was used in a range from 50 to 1,000 μ M over 30 min. The DTNB cell-impermeable reagent used to induce cysteine oxidation was obtained from Sigma-Aldrich (#D218200) and was used at 100 μ M over 30 min. Cell-impermeable Amplex red reagent (10-acetyl-3,7-dihydroxyphenoxazine) was obtained from Thermo Fisher Scientific (#A22188) and was used to detect extracellular H₂O₂. Gelatin was prepared using Bio-Gel P-30 Gel (Bio-Rad; #150-4154) and gelatin from porcine skin (Sigma-Aldrich; #G2500). The siRNAs ON-TARGETplus SMARTpool were purchased from Dharmacon and are detailed in Data S1. All siRNAs were transfected by Jet prime (Polyplus transfection) following the standard protocol. Knockdown was performed via two rounds (three for MYO1C) of siRNA transfection at 24-h intervals.

Plasmids

pcDNA-YFP TRPV4 and pcDNA-TRPM5-GFP, pcDNA-TRPM8-YFP, pcDNA-TRPA1-GFP, and pcDNA-TRPV2-CFP vectors were provided by Prof. Dr. M.A. Valverde (Laboratory of Molecular Physiology, Department of Experimental and Health Sciences, Universitat Pompeu Fabra, Barcelona, Spain). pBabeTagRFP vector was used to subclone the human TRPV4^{WT} and mutated forms E797K, 121AAWAA, Δ PRD, and M680D. Genetically encoded calcium indicator pN1 Lck-GCaMP5G was a gift from Baljit Khakh (Addgene plasmid #34924). The latter was used to

produce the following plasmids: pBabe-TRPV4-Gcamp5-GFP, pBabe-TRPV4-R269C-Gcamp5-GFP, pBabe-TRPV4-Cys294-353-457Ala-GCamp5, pBabe-TRPV4-R269C/Cys294-353-457Ala-GCamp5, pBabe-TRPV4-Cys639-645-652-660Ala-GCamp5, and pBabe-TRPV4-R269C-Cys639-645-652-660Ala-GCamp5. The ratiometric, genetically encoded H₂O₂ sensor pC1-HyPer-3 was a gift from Vsevolod Belousov (Addgene plasmid #42131), and it was used to clone pC1-Hyper-3-Paxillin and pC1-Hyper-3-GPI. pEGFP-GIT1 was a gift from Rick Horwitz (Addgene plasmid #15226), Unconventional MYO1C YFP was a gift from Primal de Lanerolle (Addgene plasmid #60241), and pcDNA3.1-MAP3K5 (WT) was a gift from Yardena Samuels (Addgene plasmid #47104). *Mus musculus* SrcY527F mutant was cloned into a pMX retroviral vector (Destaing et al., 2010). MT1-MMPmCherry and MT1-MMPpHluorin constructs were kindly provided by Prof. Dr. P. Chavrier. The detailed primers used for cloning in listed in Data S1.

Cell culture, infection, and silencing experiments

TRPV4^{-/-} MEF cells and TRPV4^{+/+} were kindly provided by Prof. Dr. M.A. Valverde. Fibroblasts were isolated from mice from the age of embryonic day 12 to postnatal day 1 as described recently (Destaing et al., 2010). Cells were grown in DMEM (containing glutamine) + 10% FBS + 1% penicillin/streptomycin supplement. cDNAs were delivered via a retroviral transduction after packaging in Phoenix-Eco cells or Phoenix-Ampho cells (American Type Culture Collection). Supernatant containing viral particles from such cells was harvested and filtered and, after the addition of 8 µg/ml polybrene (Sigma-Aldrich), was used to transduce fibroblasts. MEF cells expressing a constitutively active mutant of Src, SrcY527F, were produced as described previously (Destaing et al., 2010). The cell lines and the HEK293 cells were maintained in DMEM supplemented with 10% FCS and 1% penicillin/streptomycin. In TRPV4^{-/-} MEF-YF cells, re-expression experiments were performed via retroviral infection using pBabe vectors to express TRPV4^{WT} and mutated forms E797K, I21AAWAA, ΔPRD, and M680D; and TRPV4-Gcamp5-GFP, TRPV4 R269C-Gcamp5-GFP, TRPV4-Cys294-353-457Ala-GCamp5, TRPV4-R269C/Cys294-353-457Ala-GCamp5, TRPV4-Cys639-645-652-660Ala-GCamp5, and TRPV4-R269C-Cys639-645-652-660Ala-GCamp5 mutants. In most experiments, cDNAs were delivered via retroviral transduction after packaging in Phoenix-Eco or Phoenix-Ampho cells. For transient transfections, constructs were delivered with Jet prime (Polyplus) according to the manufacturer's instructions. MEF-SrcY527F (10⁵) cells were plated 24 h before transfection in 2-well cell culture Lab-Tek chambers or in 24-well plates with 12-mm coverslips.

Immunofluorescence microscopy, live-imaging, and FRAP

Cells were fixed for 10 min with 4% PFA in PBS, permeabilized for 10 min (0.2% Triton X-100), and blocked for 10 min in 4% BSA in PBS. Cells were then incubated for 1 h at RT with primary antibodies. For specific staining of MT1-MMP and β-integrins 1 and 3 at the plasma membrane, cells were incubated with primary antibody without any previous permeabilization. Secondary antibodies were then added for 1 h at RT. Coverslips were permanently mounted in Mowiol (EMD Millipore) containing

DAPI. Imaging of fixed cells was performed on an Apotome microscope (semi-confocal, Zeiss AxioImager Z1, AxioCam MRm camera, and AxioVision software) equipped with Plan-Apochromat (63×, NA 1.4, oil, Ph3, WD 190) objective. The images were then processed with Fiji software. For quantitative confocal imaging, all images were acquired with the same optical path and setup detection and were quantified without any ImageJ processing. For live imaging, LifeAct-TagRFP-expressing cells were seeded overnight at subconfluent densities in a serum-coated Lab-Tek coverglass. During imaging, cells were placed on a heated 37°C stage (Zeiss) with a CO₂-independent medium (18045-088; Life Technologies) and imaged with an Axiovert 200M microscope (Zeiss) equipped with a Coolsnap HQ2 camera (Photometrics) and a Plan Neo-Fluor (40X, NA 1.2) objective. Images were sampled with MetaMorph software (Molecular Devices). Time-lapse videos were then processed with ImageJ software. TIRF microscopy was performed with an Axiovert 200M microscope equipped with a Coolsnap HQ2 camera, Plan Apochromat (100×, NA 1.4, oil) objective, and a TIRF 1 slider (Zeiss). Images were acquired with MetaMorph software and processed with Fiji software. To quantify invadosome speed, surfaces delimited by invadosome rings were threshold based on the fluorescence intensity of F-actin content (fluorescent LifeAct). Then, the center of mass of this surface was defined by ImageJ (National Institutes of Health), and the process was repeated on our live-imaging data in order to measure the time necessary to observe the displacement of at least the equivalent of two identical surfaces (defining a full cycle of assembly/disassembly of a ring).

FACS analysis

Cells were quickly washed with cold PBS and scrapped before being fixed for 10 min with 4% PFA in PBS. After a 10-min block in 4% BSA in PBS, cells were then incubated for 1 h at RT with primary antibodies without any previous permeabilization. Secondary antibodies were then added for 1 h at RT. Cells were then postfixed for 10 min with 4% PFA in PBS in order to stabilize the indicated surface staining. Fluorescence of cells was analyzed with ACCURI-C6 (BD Biosciences) in order to quantify the median of fluorescence for each condition through the software C-flow (BD Biosciences). On average, 8,000 cells were analyzed per condition in three to six different experiments.

ECM degradation assay

The ECM degradation assay was performed as described previously (Sharma et al., 2013). Briefly, 12-mm coverslips in 24-well plates were coated with 50 µg/ml Poly L lysine for 20 min at RT, than with 0.25% glutaraldehyde for 15 min at 4°C, and finally with mix of 0.2% unlabeled gelatin dissolved in PBS and Alexa Fluor 647-gelatin in a 4:1 ratio for 10 min at RT and washed with PBS, medium with serum, and 70% ethanol. The cells were seeded on these gelatin-coated coverslips for 6 or 24 h, fixed, and observed with a semi-confocal microscope (AxioImager Z1, AxioCam MRm (N/B) camera, and AxioVision software) equipped with Plan-Apochromat (63×, NA 1.4, oil, Ph3, WD 190 objective). The quantification of cells' degradation ability was established by calculating the percentage of total degradation area per field

of view after setting a low-intensity threshold on gelatin-captured images and dividing by the number of cells using Fiji software.

Western blotting

Whole-cell lysates were prepared in buffer containing 50 mM Tris-HCl, pH 7.4, 150 mM NaCl, 0.5% Triton X-100, 0.5% (wt/vol) sodium deoxycholate, 1 mM NaF, 2 mM MgCl₂, 1 mM orthovanadate (Na₃VO₄), and 4% (vol/vol) protease inhibitor cocktail (complete EDTA-free; Roche Diagnostics). 30 µg of proteins from each cell lysate was subjected to SDS-PAGE, transferred to nitrocellulose membranes, and probed with primary antibodies. Immunological detection was achieved with HRP-conjugated goat anti-mouse or goat anti-rabbit secondary antibody. Peroxidase activity was visualized by ECL (West Pico Signal; Thermo Fisher Scientific) using a ChemiDoc MP imaging system (Bio-Rad Laboratories). Densitometric quantification of the bands was performed using Image Lab (Bio-Rad Laboratories). As a control, detection of actin was also performed. Stripping was performed in 60 mM Tris, pH 6.8, 2% SDS, and 100 mM β-mercaptoethanol solution and incubated at 50°C for 30 min, washed three times, and resaturated before probing with anti-Src and anti-STAT3. For quantification of pASK1, the values were normalized to the total ASK1 band.

Real-time qPCR

Total RNA was isolated using the NucleoSpin RNA II kit (MACHEREY-NAGEL) according to the manufacturer's instructions. 1 µg RNA was reverse-transcribed using the SuperScript VILO kit (Thermo Fisher Scientific). PCR amplification of cDNA from the reverse transcription reaction was performed using specific primer pairs for mouse *trpv4* (forward: 5'-CGTCCAAACCTGCGAATGAAGTTC-3'; reverse: 5'-CCTCCATCTCTTGTTGCTACTGG-3'); mouse *ASK1* (forward: 5'-AGCCTGTGCTAATGACTTGCT-3'; reverse: 5'-CTGCTGGTGTCTTCTACCAGG-3'); mouse *Ataxinlike* (forward: 5'-GTTTATTGGGTCTCCATACAGCC-3'; reverse: 5'-ACAAAGTGTGGAAGGTGAGTG-3'); mouse *Zol* (forward: 5'-GAGCGGGCTACCTTACTGAAC-3'; reverse: 5'-GTCATCTCTTCCGAGGCATTAG-3'); mouse *MYO1C* (forward: 5'-TAGTCTCTGTCAATCCCTACCG-3'; reverse: 5'-GACGCTCAGTACGAAGTGC-3'); and mouse *MMP14* (forward: 5'-CTTCGTGTTGCTGATGAC-3'; reverse: 5'-GTTATTCTCACCAGCCAGA-3'). Real-time qPCR was performed with GoTaq QPCR Master Mix (Promega) in a 25-µl reaction on a thermal cycler (C-1000 Touch; Bio-Rad Laboratories). Ct values were determined with the same software, and normalization was conducted with the housekeeping genes *actin*, *RanBP1*, *GAPDH*, and *HPRT*, which yielded similar results. The expression levels of each target gene in the siRNA-treated cells were calculated with GAPDH as a reference gene and compared with the controls.

Immunoprecipitation

MEF-SrcY527F TRPV4^{-/-} stably expressing or not tgRFP-TRPV4^{WT} were washed with cold PBS, passed six times through the GA26 syringe, incubated 20 min on ice in lysis buffer containing 100 mM NaCl 1% NP-40, 0.5% Na DOC, 50 mM Tris, pH7.4, 1X proteases inhibitors (Roche Diagnostics), 1 mM

Na orthovanadate, 10 mM Na fluoride, and 10 mM glycerophosphate, and then incubated under rotation for 30 min at 4°C. The cell debris was then removed by centrifugation at 5,000 rpm for 10 min at 4°C. Cell lysates were precleared using IgG Sepharose beads (GE Healthcare) for 30 min under rotation at 4°C. The supernatant was collected and incubated with α-Tag RFP (Evrogen; 5 µg of antibody for 0.5 mg protein) under rotation for 2 h at 4°C. Beads that contained tag-RFP proteins were washed three times with the lysis buffer. After centrifugation, the pellets were subjected to SDS-PAGE and silver staining for protein detection. The same samples were also used for proteomic analyses. The interaction of endogenous ASK1 and TRPV4 was confirmed by Western blot staining using α-ASK1 (mouse; Santa Cruz), and the expression of tag-RFP TRPV4 was confirmed in the same blots using α-tagRFP.

Mass spectrometry-based proteomic analyses and network analysis

Proteins eluted from coIP using Laemmli buffer were separated by SDS-PAGE (NuPAGE 4%–12%; Invitrogen) before being stained with Coomassie blue R-250 (Bio-Rad Laboratories). Proteins were then in-gel digested using modified trypsin (sequencing grade; Promega) as previously described (Salveti et al., 2016). Resulting peptides were analyzed by online nano-liquid chromatography coupled to tandem mass spectrometry (UltiMate 3000 and LTQ-Orbitrap Velos Pro; Thermo Fisher Scientific). Peptides were sampled on a 300 µm × 5 mm PepMap C18 precolumn and separated on a 75 µm × 250 mm C18 column (PepMap; Thermo Fisher Scientific) using a 120-min gradient. Mass spectrometry and tandem mass spectrometry data were acquired using Xcalibur (Thermo Fisher Scientific). Peptides and proteins were identified using Mascot (version 2.6) through concomitant searches against Uniprot (*M. musculus* taxonomy), classical contaminants database (homemade), and the corresponding reversed databases. Proline software was used to filter the results: conservation of rank 1 peptides, peptide identification false discovery rate <1% as calculated on peptide scores by using the reverse database strategy, and minimum of one specific peptide per identified protein group. Proline was then used to perform compilation, grouping, and spectral counting-based comparison of the protein groups identified in the different samples. Proteins from the contaminant database and keratins were discarded from the final list of identified proteins. Only proteins identified with at least two specific spectral counts only in Trpv4 coIP or enriched at least three times in Trpv4 coIP compared with negative control (KO) coIP were considered as potential Trpv4-binding partners.

We reconstructed the protein–protein interaction network by gathering BIOGRID, INTACT, and MINT protein–protein interaction data from *Homo sapiens* with PSIQUIC retrieval (07122017) and cytoscape environment. To acknowledge protein functions, gene ontologies (GOs) were gathered for ROS signaling in the Quickgo platform (<https://www.ebi.ac.uk/QuickGO/>; GO IDs: GO:0006979 and GO:1901700 and their respective child terms), as well as from the literature. On the other hand, due to their large number of referring terms, proteins involved in calcium signaling were instead collected from the Uniprot

database, selecting human proteins according to “calcium” keyword, as well as from a thorough literature survey.

Statistical analysis

Quantitative data are presented as means \pm SEM and were statistically analyzed using a two-sided unpaired *t* test (PRISM software). Based on the numerous measurements for each condition, data distributions were assumed to be normal, but this was not formally tested each time. Differences with a probability level <0.05 were considered significant. All graphs include SD or SEM error bars.

Online supplemental material

Fig. S1 localizes TRPV4 and other TRPs in invadosomes. **Fig. S2** shows that TRPV4 regulates the dynamics of the acto-adhesive functions of invadosomes and their ability to digest ECM. **Fig. S3** demonstrates that TRPV4 is also a regulator of acto-adhesion and ADC in podosomes of the macrophage cell line RAW264.7. **Fig. S4** shows structure-function studies that revealed the importance of calcium permeation and the adaptor functions of TRPV4 on TRPV4 localization and its regulation of invadosomes. **Fig. S5** characterizes the effects of ASK1 and MYO1C on invadosomes. **Fig. S6** illustrates invadosome responses to the cell-permeable oxidant H_2O_2 and the extracellular oxidant DTNB. **Fig. S7** characterizes Gcamp-TRPV4^{WT} and Gcamp-TRPV4 mutants of extra- and intracellular stretches of cysteines that rescue the activity of a pathological cysteine mutation (TRPV4R269C). Data S1 describes the constructs, siRNA mixes, and antibodies used in this study. It also contains additional controls, localization, representation of time series, and characterization of TRPV4 mutants used.

Acknowledgments

We would like to acknowledge Dr. A. Penna for critical reading of this manuscript and exciting discussions.

This work was funded by the Agence Nationale de la Recherche (ANR; invadocontrol; ANR-13-JSV2-0003-01) program and Ligue Contre le Cancer as “Equipe labellisée Ligue 2014” (EL2014.LNCC/CAR) the Spanish Ministry of Economy, Industry, and Competitiveness through grant RTI2018-099718, the institutional “Maria de Maeztu” Program for Units of Excellence in Research and Development, and FEDER funds. S. Vellino was funded by the ANR, ARC Foundation, and European Marie-Sklodowska-Curie funding program. We are thankful for the support of the discovery platform and informatics group at EDyP. Proteomic experiments were partly supported by the Proteomics French Infrastructure (grant ANR-10-INBS-08-01) and Labex GRAL (grant ANR-10-LABX-49-01).

The authors declare no competing financial interests.

Author contributions: S. Vellino was involved in conceptualization, formal analysis, funding acquisition, investigation, methodology, supervision, and writing of the original draft. C. Oddou, E. Hiriart-Bryant, and P. Rivier were involved in methodology, formal analysis, and investigation. C. Boyault was involved in methodology and visualization. A. Kraut was involved in formal analysis, investigation, and curation. R. Martin

was involved in resources. Y. Coute was involved in formal analysis, investigation, curation, and writing (review and editing). H.-J. Knölker was involved in resources and writing (review and editing). M.A. Valverde was involved in resources, supervision, and writing (review and editing). C. Albigès-Rizo was involved in funding acquisition, supervision, and writing (review and editing). O. Destaing was involved in conceptualization, formal analysis, funding acquisition, investigation, methodology, project administration, supervision, validation, visualization, and writing (original draft, review and editing).

Submitted: 12 October 2019

Revised: 23 July 2020

Accepted: 13 November 2020

References

- Agidigbi, T.S., and C. Kim. 2019. Reactive Oxygen Species in Osteoclast Differentiation and Possible Pharmaceutical Targets of ROS-Mediated Osteoclast Diseases. *Int. J. Mol. Sci.* 20:3576. <https://doi.org/10.3390/ijms20143576>
- Alessandri-Haber, N., O.A. Dina, E.K. Joseph, D.B. Reichling, and J.D. Levine. 2008. Interaction of transient receptor potential vanilloid 4, integrin, and SRC tyrosine kinase in mechanical hyperalgesia. *J. Neurosci.* 28: 1046–1057. <https://doi.org/10.1523/JNEUROSCI.4497-07.2008>
- Banfi, G., E.L. Iorio, and M.M. Corsi. 2008. Oxidative stress, free radicals and bone remodeling. *Clin. Chem. Lab. Med.* 46:1550–1555. <https://doi.org/10.1515/CCLM.2008.302>
- Beaty, B.T., V.P. Sharma, J.J. Bravo-Cordero, M.A. Simpson, R.J. Eddy, A.J. Koleske, and J. Condeelis. 2013. $\beta 1$ integrin regulates Arg to promote invadopodial maturation and matrix degradation. *Mol. Biol. Cell.* 24: 1661–1675, S1–S11. <https://doi.org/10.1091/mbc.e12-12-0908>
- Bilan, D.S., L. Pase, L. Joosen, A.Y. Gorokhovovskiy, Y.G. Ermakova, T.W.J. Gadella, C. Grabher, C. Schultz, S. Lukyanov, and V.V. Belousov. 2013. HyPer-3: a genetically encoded H(2)O(2) probe with improved performance for ratiometric and fluorescence lifetime imaging. *ACS Chem. Biol.* 8:535–542. <https://doi.org/10.1021/cb300625g>
- Bizzarro, V., A. Petrella, and L. Parente. 2012. Annexin A1: novel roles in skeletal muscle biology. *J. Cell. Physiol.* 227:3007–3015. <https://doi.org/10.1002/jcp.24032>
- Boateng, L.R., and A. Huttenlocher. 2012. Spatiotemporal regulation of Src and its substrates at invadosomes. *Eur. J. Cell Biol.* 91:878–888. <https://doi.org/10.1016/j.ejcb.2012.06.003>
- Bond, L.M., H. Brandstaetter, J. Kendrick-Jones, and F. Buss. 2013. Functional roles for myosin 1c in cellular signaling pathways. *Cell. Signal.* 25: 229–235. <https://doi.org/10.1016/j.cellsig.2012.09.026>
- Branch, K.M., D. Hoshino, and A.M. Weaver. 2012. Adhesion rings surround invadopodia and promote maturation. *Biol. Open.* 1:711–722. <https://doi.org/10.1242/bio.20121867>
- Bubolz, A.H., S.A. Mendoza, X. Zheng, N.S. Zinkevich, R. Li, D.D. Gutterman, and D.X. Zhang. 2011. Activation of endothelial TRPV4 channels mediates flow-induced dilation in human coronary arterioles: role of Ca 2+ entry and mitochondrial ROS signaling. *Am. J. Physiol. Circ. Physiol.* 302: H634–H642. <https://doi.org/10.1152/ajpheart.00717.2011>
- Buschman, M.D., P.A. Bromann, P. Cejudo-Martin, F. Wen, I. Pass, and S.A. Courtneidge. 2009. The novel adaptor protein Tks4 (SH3PXD2B) is required for functional podosome formation. *Mol. Biol. Cell.* 20: 1302–1311. <https://doi.org/10.1091/mbc.e08-09-0949>
- Chiarugi, P., G. Pani, E. Giannoni, L. Taddei, R. Colavitti, G. Raugei, M. Symons, S. Borrello, T. Galeotti, and G. Ramponi. 2003. Reactive oxygen species as essential mediators of cell adhesion: the oxidative inhibition of a FAK tyrosine phosphatase is required for cell adhesion. *J. Cell Biol.* 161:933–944. <https://doi.org/10.1083/jcb.200211118>
- Chung, C.L., S.W. Wang, R. Martin, H.J. Knölker, Y.C. Kao, M.H. Lin, J.J. Chen, Y.B. Huang, D.C. Wu, and C.L. Chen. 2018. Pentachloropseudilin Inhibits Transforming Growth Factor- β (TGF- β) Activity by Accelerating Cell-Surface Type II TGF- β Receptor Turnover in Target Cells. *Chem-BioChem.* 19:851–864. <https://doi.org/10.1002/cbic.201700693>
- Clark, K., M. Langeslag, B. van Leeuwen, L. Ran, A.G. Ryazanov, C.G. Figdor, W.H. Moolenaar, K. Jalink, and F.N. van Leeuwen. 2006. TRPM7, a

- novel regulator of actomyosin contractility and cell adhesion. *EMBO J.* 25:290–301. <https://doi.org/10.1038/sj.emboj.7600931>
- de Rezende, F.F., A. Martins Lima, S. Niland, I. Wittig, H. Heide, K. Schröder, and J.A. Eble. 2012. Integrin $\alpha 7 \beta 1$ is a redox-regulated target of hydrogen peroxide in vascular smooth muscle cell adhesion. *Free Radic. Biol. Med.* 53:521–531. <https://doi.org/10.1016/j.freeradbiomed.2012.05.032>
- Destaing, O., F. Saltel, J.C. Géminard, P. Jurdic, and F. Bard. 2003. Podosomes display actin turnover and dynamic self-organization in osteoclasts expressing actin-green fluorescent protein. *Mol. Biol. Cell.* 14:407–416. <https://doi.org/10.1091/mbc.e02-07-0389>
- Destaing, O., E. Planus, D. Bouvard, C. Oddou, C. Badowski, V. Bossy, A. Raducanu, B. Fourcade, C. Albigès-Rizo, and M.R. Block. 2010. $\beta 1 A$ integrin is a master regulator of invadosome organization and function. *Mol. Biol. Cell.* 21:4108–4119. <https://doi.org/10.1091/mbc.e10-07-0580>
- Diaz, B., G. Shani, I. Pass, D. Anderson, M. Quintavalle, and S.A. Courtneidge. 2009. Tks5-dependent, nox-mediated generation of reactive oxygen species is necessary for invadopodia formation. *Sci. Signal.* 2:ra53. <https://doi.org/10.1126/scisignal.2000368>
- Donnelly, S.K., R. Cabrera, S.P.H. Mao, J.R. Christin, B. Wu, W. Guo, J.J. Bravo-Cordero, J.S. Condeelis, J.E. Segall, and L. Hodgson. 2017. Rac3 regulates breast cancer invasion and metastasis by controlling adhesion and matrix degradation. *J. Cell Biol.* 216:4331–4349. <https://doi.org/10.1083/jcb.201704048>
- Franco, S.J., M.A. Rodgers, B.J. Perrin, J. Han, D.A. Bennin, D.R. Critchley, and A. Huttenlocher. 2004. Calpain-mediated proteolysis of talin regulates adhesion dynamics. *Nat. Cell Biol.* 6:977–983. <https://doi.org/10.1038/ncb1175>
- García-Elias, A., I.M. Lorenzo, R. Vicente, and M.A. Valverde. 2008. IP3 receptor binds to and sensitizes TRPV4 channel to osmotic stimuli via a calmodulin-binding site. *J. Biol. Chem.* 283:31284–31288. <https://doi.org/10.1074/jbc.C800184200>
- García-Elias, A., S. Mrkonjić, C. Pardo-Pastor, H. Inada, U.A. Hellmich, F. Rubio-Moscardó, C. Plata, R. Gaudet, R. Vicente, and M.A. Valverde. 2013. Phosphatidylinositol-4,5-bisphosphate-dependent rearrangement of TRPV4 cytosolic tails enables channel activation by physiological stimuli. *Proc. Natl. Acad. Sci. USA.* 110:9553–9558. <https://doi.org/10.1073/pnas.1220231110>
- García-Elias, A., S. Mrkonjić, C. Jung, C. Pardo-Pastor, R. Vicente, and M.A. Valverde. 2014. The TRPV4 channel. *Handb. Exp. Pharmacol.* 222: 293–319. https://doi.org/10.1007/978-3-642-54215-2_12
- Gianni, D., B. Diaz, N. Taulet, B. Fowler, S.A. Courtneidge, and G.M. Bokoch. 2009. Novel p47(phox)-related organizers regulate localized NADPH oxidase 1 (Nox1) activity. *Sci. Signal.* 2:ra54. <https://doi.org/10.1126/scisignal.2000370>
- Gianni, D., N. Taulet, C. DerMardirossian, and G.M. Bokoch. 2010. c-Src-mediated phosphorylation of Nox1 and Tks4 induces the reactive oxygen species (ROS)-dependent formation of functional invadopodia in human colon cancer cells. *Mol. Biol. Cell.* 21:4287–4298. <https://doi.org/10.1091/mbc.e10-08-0685>
- Giannoni, E., F. Buricchi, G. Raugei, G. Ramponi, and P. Chiarugi. 2005. Intracellular reactive oxygen species activate Src tyrosine kinase during cell adhesion and anchorage-dependent cell growth. *Mol. Cell. Biol.* 25: 6391–6403. <https://doi.org/10.1128/MCB.25.15.6391-6403.2005>
- Giannoni, E., M.L. Taddei, and P. Chiarugi. 2010. Src redox regulation: again in the front line. *Free Radic. Biol. Med.* 49:516–527. <https://doi.org/10.1016/j.freeradbiomed.2010.04.025>
- Gilchrist, C.L., H.A. Leddy, L. Kaye, N.D. Case, K.E. Rothenberg, D. Little, W. Liedtke, B.D. Hoffman, and F. Guilak. 2019. TRPV4-mediated calcium signaling in mesenchymal stem cells regulates aligned collagen matrix formation and vinculin tension. *Proc. Natl. Acad. Sci. USA.* 116:1992–1997. <https://doi.org/10.1073/pnas.1811095116>
- Greenberg, M.J., T. Lin, Y.E. Goldman, H. Shuman, and E.M. Ostap. 2012. Myosin IC generates power over a range of loads via a new tension-sensing mechanism. *Proc. Natl. Acad. Sci. USA.* 109:E2433–E2440. <https://doi.org/10.1073/pnas.1207811109>
- Groen, A., J. Overvoorde, T. van der Wijk, and J. den Hertog. 2008. Redox regulation of dimerization of the receptor protein-tyrosine phosphatases RPTPalpha, LAR, RPTPmu and CD45. *FEBS J.* 275:2597–2604. <https://doi.org/10.1111/j.1742-4658.2008.06407.x>
- Hattori, K., I. Naguro, C. Runchel, and H. Ichijo. 2009. The roles of ASK family proteins in stress responses and diseases. *Cell Commun. Signal.* 7:9. <https://doi.org/10.1186/1478-811X-7-9>
- Hellmich, U.A., and R. Gaudet. 2014. Structural biology of TRP channels. *Handb. Exp. Pharmacol.* 223:963–990. https://doi.org/10.1007/978-3-319-05161-1_10
- Hong, Z., Y. Tian, Y. Yuan, M. Qi, Y. Li, Y. Du, L. Chen, and L. Chen. 2016. Enhanced Oxidative Stress Is Responsible for TRPV4-Induced Neurotoxicity. *Front. Cell. Neurosci.* 10:232. <https://doi.org/10.3389/fncel.2016.00232>
- Huynh, K.W., M.R. Cohen, S. Chakrapani, H.A. Holdaway, P.L. Stewart, and V.Y. Moiseenkova-Bell. 2014. Structural insight into the assembly of TRPV channels. *Structure.* 22:260–268. <https://doi.org/10.1016/j.str.2013.11.008>
- Infante, E., A. Castagnino, R. Ferrari, P. Monteiro, S. Agüera-González, P. Paul-Gilloteaux, M.J. Domingues, P. Maiuri, M. Raab, C.M. Shanahan, et al. 2018. LINC complex-Lis1 interplay controls MT1-MMP matrix digest-on-demand response for confined tumor cell migration. *Nat. Commun.* 9:2443. <https://doi.org/10.1038/s41467-018-04865-7>
- Kashiwase, K., Y. Higuchi, S. Hirotsu, O. Yamaguchi, S. Hikoso, T. Takeda, T. Watanabe, M. Taniike, A. Nakai, I. Tsujimoto, et al. 2005. CaMKII activates ASK1 and NF-kappaB to induce cardiomyocyte hypertrophy. *Biochem. Biophys. Res. Commun.* 327:136–142. <https://doi.org/10.1016/j.bbrc.2004.12.002>
- Kelley, L.C., A.G. Ammer, K.E. Hayes, K.H. Martin, K. Machida, L. Jia, B.J. Mayer, and S.A. Weed. 2010. Oncogenic Src requires a wild-type counterpart to regulate invadopodia maturation. *J. Cell Sci.* 123: 3923–3932. <https://doi.org/10.1242/jcs.075200>
- Kemble, D.J., and G. Sun. 2009. Direct and specific inactivation of protein tyrosine kinases in the Src and FGFR families by reversible cysteine oxidation. *Proc. Natl. Acad. Sci. USA.* 106:5070–5075. <https://doi.org/10.1073/pnas.0806117106>
- Kishimoto, E., Y. Naito, O. Handa, H. Okada, K. Mizushima, Y. Hirai, N. Nakabe, K. Uchiyama, T. Ishikawa, T. Takagi, et al. 2011. Oxidative stress-induced posttranslational modification of TRPV1 expressed in esophageal epithelial cells. *Am. J. Physiol. Gastrointest. Liver Physiol.* 301: G230–G238. <https://doi.org/10.1152/ajpgi.00436.2009>
- Knowles, T.P.J., M. Vendruscolo, and C.M. Dobson. 2014. The amyloid state and its association with protein misfolding diseases. *Nat. Rev. Mol. Cell Biol.* 15:384–396. <https://doi.org/10.1038/nrm3810>
- Kozai, D., Y. Kabasawa, M. Ebert, S. Kiyonaka, Y. Otani, T. Numata, N. Takahashi, Y. Mori, and T. Ohwada. 2014. Transnitrosylation directs TRPA1 selectivity in N-nitrosamine activators. *Mol. Pharmacol.* 85:175–185. <https://doi.org/10.1124/mol.113.088864>
- Labernadie, A., A. Bouissou, P. Delobelle, S. Balor, R. Voituriez, A. Proag, I. Fourquaux, C. Thibault, C. Vieu, R. Poincloux, et al. 2014. Protrusion force microscopy reveals oscillatory force generation and mechanosensing activity of human macrophage podosomes. *Nat. Commun.* 5: 5343. <https://doi.org/10.1038/ncomms6343>
- Leisner, T.M., T.C. Freeman, J.L. Black, and L.V. Parise. 2016. CIB1: a small protein with big ambitions. *FASEB J.* 30:2640–2650. <https://doi.org/10.1096/fj.201500073R>
- Loukin, S.H., J. Teng, and C. Kung. 2015. A channelopathy mechanism revealed by direct calmodulin activation of TrpV4. *Proc. Natl. Acad. Sci. USA.* 112:9400–9405. <https://doi.org/10.1073/pnas.1510602112>
- Mallawaarachy, D.M., M.E. Buckland, K.L. McDonald, C.C.Y. Li, L. Ly, E.K. Sykes, R.I. Christopherson, and K.L. Kaufman. 2015. Membrane proteome analysis of glioblastoma cell invasion. *J. Neuropathol. Exp. Neurol.* 74:425–441. <https://doi.org/10.1097/NEN.0000000000000187>
- Maly, I.V., and W.A. Hofmann. 2016. Calcium-regulated import of myosin IC into the nucleus. *Cytoskeleton (Hoboken)*. 73:341–350. <https://doi.org/10.1002/cm.21310>
- Marengo, B., M. Nitti, A.L. Furfaro, R. Colla, C.D. Ciucis, U.M. Marinari, M.A. Pronzato, N. Traverso, and C. Domenicotti. 2016. Redox Homeostasis and Cellular Antioxidant Systems: Crucial Players in Cancer Growth and Therapy. *Oxid. Med. Cell. Longev.* 2016:6235641. <https://doi.org/10.1155/2016/6235641>
- Martin, R., A. Jäger, M. Böhl, S. Richter, R. Fedorov, D.J. Manstein, H.O. Gutzeit, and H.J. Knölker. 2009. Total synthesis of pentabromo- and pentachloropseudilin, and synthetic analogues—allosteric inhibitors of myosin ATPase. *Angew. Chem. Int. Ed. Engl.* 48:8042–8046. <https://doi.org/10.1002/anie.200903743>
- Masuyama, R., A. Mizuno, H. Komori, H. Kajijiya, A. Uekawa, H. Kitaura, K. Okabe, K. Ohyama, and T. Komori. 2012. Calcium/calmodulin-signaling supports TRPV4 activation in osteoclasts and regulates bone mass. *J. Bone Miner. Res.* 27:1708–1721. <https://doi.org/10.1002/jbmr.1629>
- Matthews, B.D., C.K. Thodeti, J.D. Tytell, A. Mammoto, D.R. Overby, and D.E. Ingber. 2010. Ultra-rapid activation of TRPV4 ion channels by mechanical forces applied to cell surface $\beta 1$ integrins. *Integr. Biol.* 2: 435–442. <https://doi.org/10.1039/c0ib00034e>
- Milloud, R., O. Destaing, R. de Mets, I. Bourrin-Reynard, C. Oddou, A. Delon, I. Wang, C. Albigès-Rizo, and M. Balland. 2017. $\alpha v \beta 3$ integrins negatively regulate cellular forces by phosphorylation of its distal NPXY site. *Biol. Cell.* 109:127–137. <https://doi.org/10.1111/boc.201600041>

- Moore, C., and W.B. Liedtke. 2017. Osmomechanical-sensitive TRPV channels in mammals. *In* Neurobiology of TRP Channels. T.L.R. Emir, editor. CRC Press/Taylor & Francis, Boca Raton, FL. Chapter 5.
- Mrkonjić, S., A. Garcia-Elias, C. Pardo-Pastor, E. Bazellières, X. Trepast, J. Vriens, D. Ghosh, T. Voets, R. Vicente, and M.A. Valverde. 2015. TRPV4 participates in the establishment of trailing adhesions and directional persistence of migrating cells. *Pflugers Arch.* 467:2107–2119. <https://doi.org/10.1007/s00424-014-1679-8>
- Nagasawa, M., and I. Kojima. 2012. Translocation of calcium-permeable TRPV2 channel to the podosome: Its role in the regulation of podosome assembly. *Cell Calcium.* 51:186–193. <https://doi.org/10.1016/j.ceca.2011.12.012>
- Nakai, J., M. Ohkura, and K. Imoto. 2001. A high signal-to-noise Ca(2+) probe composed of a single green fluorescent protein. *Nat. Biotechnol.* 19: 137–141. <https://doi.org/10.1038/84397>
- Nilius, B., and T. Voets. 2013. The puzzle of TRPV4 channelopathies. *EMBO Rep.* 14:152–163. <https://doi.org/10.1038/embor.2012.219>
- Nishida, T., K. Hattori, and K. Watanabe. 2017. The regulatory and signaling mechanisms of the ASK family. *Adv. Biol. Regul.* 66:2–22. <https://doi.org/10.1016/j.jbior.2017.05.004>
- Ogawa, N., T. Kurokawa, K. Fujiwara, O.K. Polat, H. Badr, N. Takahashi, and Y. Mori. 2016. Functional and structural divergence in human TRPV1 channel subunits by oxidative cysteine modification. *J. Biol. Chem.* 291: 4197–4210. <https://doi.org/10.1074/jbc.M115.700278>
- Pardo-Pastor, C., F. Rubio-Moscardo, M. Vogel-González, S.A. Serra, A. Afthinos, S. Mrkonjic, O. Destaing, J.F. Abenza, J.M. Fernández-Fernández, X. Trepast, et al. 2018. Piezo2 channel regulates RhoA and actin cytoskeleton to promote cell mechanobiological responses. *Proc. Natl. Acad. Sci. USA.* 115:1925–1930. <https://doi.org/10.1073/pnas.1718177115>
- Paterson, E.K., and S.A. Courtneidge. 2018. Invadosomes are coming: new insights into function and disease relevance. *FEBS J.* 285:8–27. <https://doi.org/10.1111/febs.14123>
- Petropoulos, C., C. Oddou, A. Emadali, E. Hiriart-Bryant, C. Boyault, E. Faurobert, S. Vande Pol, J.R. Kim-Kaneyama, A. Kraut, Y. Coute, et al. 2016. Roles of paxillin family members in adhesion and ECM degradation coupling at invadosomes. *J. Cell Biol.* 213:585–599. <https://doi.org/10.1083/jcb.201510036>
- Poincloux, R., O. Collin, F. Lizárraga, M. Romao, M. Debray, M. Piel, and P. Chavrier. 2011. Contractility of the cell rear drives invasion of breast tumor cells in 3D Matrigel. *Proc. Natl. Acad. Sci. USA.* 108:1943–1948. <https://doi.org/10.1073/pnas.1010396108>
- Prickett, T.D., B. Zerlanko, J.J. Gartner, S.C.J. Parker, K. Dutton-Regester, J.C. Lin, J.K. Teer, X. Wei, J. Jiang, G. Chen, et al. Nisc Comparative Sequencing Program. 2014. Somatic mutations in MAP3K5 attenuate its proapoptotic function in melanoma through increased binding to thiorodoxin. *J. Invest. Dermatol.* 134:452–460. <https://doi.org/10.1038/jid.2013.365>
- Sakurai-Yageta, M., C. Recchi, G. Le Dez, J.B. Sibarita, L. Daviet, J. Camonis, C. D'Souza-Schorey, and P. Chavrier. 2008. The interaction of IQGAP1 with the exocyst complex is required for tumor cell invasion downstream of Cdc42 and RhoA. *J. Cell Biol.* 181:985–998. <https://doi.org/10.1083/jcb.200709076>
- Salvetti, A., Y. Couté, A. Epstein, L. Arata, A. Kraut, V. Navratil, P. Bouvet, and A. Greco. 2016. Nuclear functions of nucleolin through global proteomics and interactomic approaches. *J. Proteome Res.* 15:1659–1669. <https://doi.org/10.1021/acs.jproteome.6b00126>
- Schiller, H.B., and R. Fässler. 2013. Mechanosensitivity and compositional dynamics of cell-matrix adhesions. *EMBO Rep.* 14:509–519. <https://doi.org/10.1038/embor.2013.49>
- Sharma, V.P., R. Eddy, D. Entenberg, M. Kai, F.B. Gertler, and J. Condeelis. 2013. Tks5 and SHIP2 regulate invadopodium maturation, but not initiation, in breast carcinoma cells. *Curr Biol.* 23:2079–2089. <https://doi.org/10.1016/j.cub.2013.08.044>
- Siddiqui, T.A., S. Lively, C. Vincent, and L.C. Schlichter. 2012. Regulation of podosome formation, microglial migration and invasion by Ca(2+)-signaling molecules expressed in podosomes. *J. Neuroinflammation.* 9: 250. <https://doi.org/10.1186/1742-2094-9-250>
- Stock, C., and S.F. Pedersen. 2017. Roles of pH and the Na⁺/H⁺ exchanger NHE1 in cancer: From cell biology and animal models to an emerging translational perspective? *Semin. Cancer Biol.* 43:5–16. <https://doi.org/10.1016/j.semcancer.2016.12.001>
- Sun, J., F. Lu, H. He, J. Shen, J. Messina, R. Mathew, D. Wang, A.A. Sarnaik, W.C. Chang, M. Kim, et al. 2014. STIM1- and Orail-mediated Ca(2+) oscillation orchestrates invadopodium formation and melanoma invasion. *J. Cell Biol.* 207:535–548. <https://doi.org/10.1083/jcb.201407082>
- Taddei, M.L., M. Parri, T. Mello, A. Catalano, A.D. Levine, G. Raugei, G. Ramponi, and P. Chiarugi. 2007. Integrin-mediated cell adhesion and spreading engage different sources of reactive oxygen species. *Antioxid. Redox Signal.* 9:469–481. <https://doi.org/10.1089/ars.2006.1392>
- Tang, X.D., M.L. Garcia, S.H. Heinemann, and T. Hoshi. 2004. Reactive oxygen species impair Slo1 BK channel function by altering cysteine-mediated calcium sensing. *Nat. Struct. Mol. Biol.* 11:171–178. <https://doi.org/10.1038/nsmb725>
- Thodeti, C.K., B. Matthews, A. Ravi, A. Mammoto, K. Ghosh, A.L. Bracha, and D.E. Ingber. 2009. TRPV4 channels mediate cyclic strain-induced endothelial cell reorientation through integrin-to-integrin signaling. *Circ. Res.* 104:1123–1130. <https://doi.org/10.1161/CIRCRESAHA.108.192930>
- von Wichert, G., G. Jiang, A. Kostic, K. De Vos, J. Sap, and M.P. Sheetz. 2003. RPTP- α acts as a transducer of mechanical force on α v β 3-integrin-cytoskeleton linkages. *J. Cell Biol.* 161:143–153. <https://doi.org/10.1083/jcb.200211061>
- White, J.P.M., M. Cibelli, L. Urban, B. Nilius, J.G. McGeown, and I. Nagy. 2016. TRPV4: Molecular Conductor of a Diverse Orchestra. *Physiol. Rev.* 96: 911–973. <https://doi.org/10.1152/physrev.00016.2015>
- Yang, H., L. Guan, S. Li, Y. Jiang, N. Xiong, L. Li, C. Wu, H. Zeng, and Y. Liu. 2016. Mechanosensitive caveolin-1 activation-induced PI3K/Akt/mTOR signaling pathway promotes breast cancer motility, invadopodia formation and metastasis in vivo. *Oncotarget.* 7:16227–16247. <https://doi.org/10.18632/oncotarget.7583>
- Yip, M.F., G. Ramm, M. Larance, K.L. Hoehn, M.C. Wagner, M. Guilhaus, and D.E. James. 2008. CaMKII-mediated phosphorylation of the myosin motor Myo1c is required for insulin-stimulated GLUT4 translocation in adipocytes. *Cell Metab.* 8:384–398. <https://doi.org/10.1016/j.cmet.2008.09.011>
- Yoneda, M., H. Suzuki, N. Hatano, S. Nakano, Y. Muraki, K. Miyazawa, S. Goto, and K. Muraki. 2019. PIEZO1 and TRPV4, which Are Distinct Mechano-Sensors in the Osteoblastic MC3T3-E1 Cells, Modify Cell-Proliferation. *IJMS.* 20:4960.
- Yoo, S.K., T.W. Starnes, Q. Deng, and A. Huttenlocher. 2011. Lyn is a redox sensor that mediates leukocyte wound attraction in vivo. *Nature.* 480: 109–112. <https://doi.org/10.1038/nature10632>
- Yoo, S.K., C.M. Freisinger, D.C. LeBert, and A. Huttenlocher. 2012. Early redox, Src family kinase, and calcium signaling integrate wound responses and tissue regeneration in zebrafish. *J. Cell Biol.* 199:225–234. <https://doi.org/10.1083/jcb.201203154>

Supplemental material

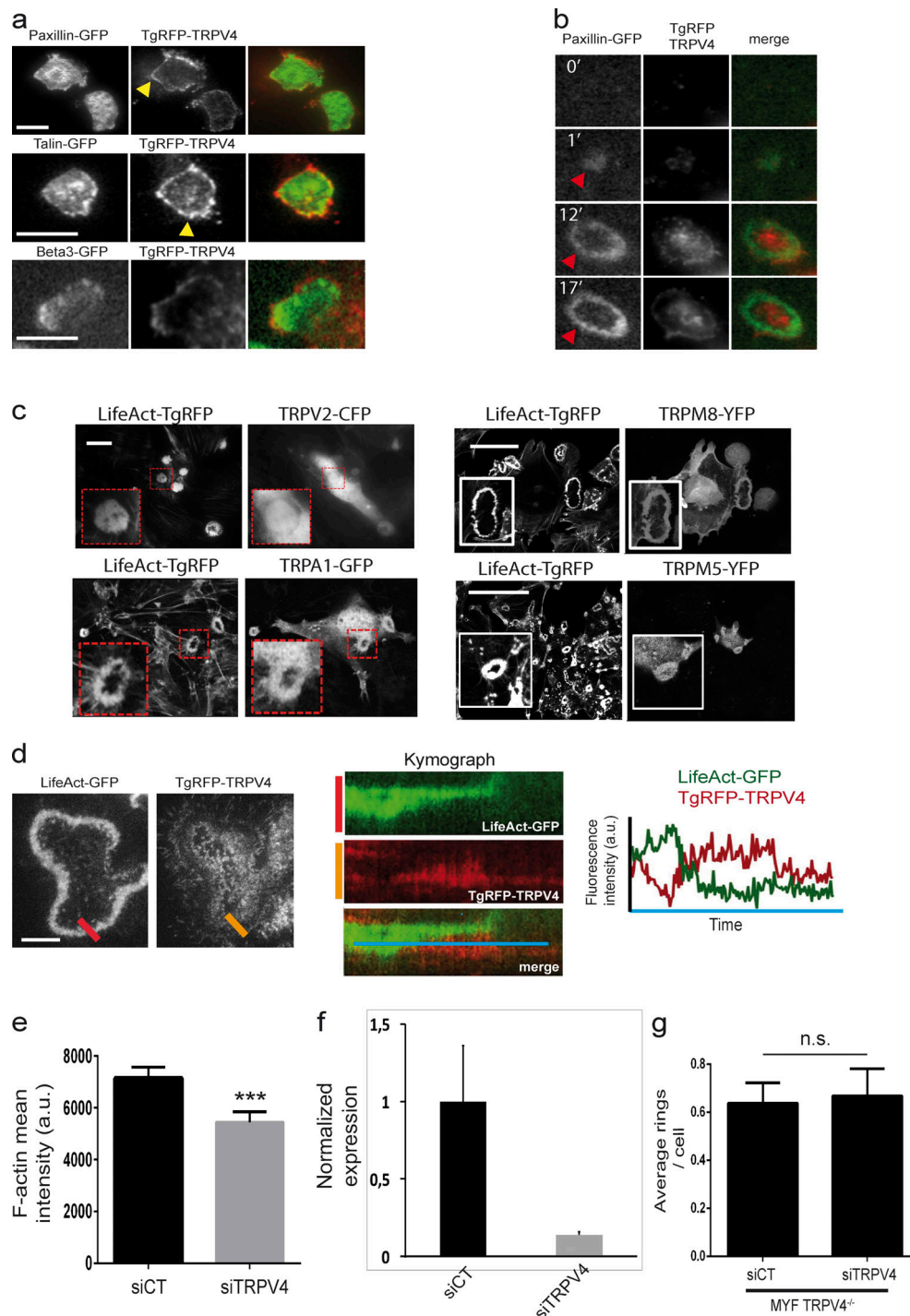


Figure S1. **Localization of TRPV4 and other TRPs in invadosomes.** (a) Representative images of MYF-TRPV4^{-/-} cells stably expressing TgRFP-TRPV4^{WT} and transfected with the following adhesive proteins: paxillin-GFP, talin-GFP, and β 3-integrin-GFP on digestible gelatin-Alexa Fluor 488. Invadosomes were observed through phalloidin-Alexa Fluor 647 staining. The yellow arrowheads indicate TgRFP-TRPV4^{WT} with the indicated adhesive proteins. (b) Representative images extracted from a time series of MYF-TRPV4^{-/-} cells stably expressing TgRFP-TRPV4^{WT} and transfected with paxillin-GFP. The red arrowheads indicate invadosome ring formation that is strictly associated with peripheral TgRFP-TRPV4^{WT} accumulation. (c) Representative images of MYF cells (zoom on an invadosome ring in red or white boxes) expressing different calcium channels (fused to fluorescent tags) close to TRPV4 or implicated previously in invadosome biology and the F-actin marker LifeAct-TgRFP. All these channels accumulated in invadosomes but did not accumulate at the invadosome periphery like TRPV4 did. (d) Kymograph analysis along red (LifeAct-RFP) and orange (YFP-TRPV4) lines in MYF cells show the transient accumulation of TRPV4 coinciding with invadosome disorganization (as shown by measuring fluorescence intensities over time; blue line). (e) Quantification of the mean intensity of F-actin of invadosomes shows that TRPV4 silencing induced a small and significant decrease in F-actin content in this structure (SEM; $n = 3$; >70 cells per condition; unpaired t test). (f) Quantification of the efficiency of TRPV4 siRNA treatments by qPCR (SEM; $n = 2$). (g) TRPV4 silencing in MYF-TRPV4^{-/-} cells did not induce a significant change in the number of invadosome rings per cell (SEM; $n = 3$; >400 cells per condition; unpaired t test) and showed the specificity of our siRNA approach. Scale bar: 5 μ m (a and b), 10 μ m (c), and 5 μ m (d). n.s., not significant.

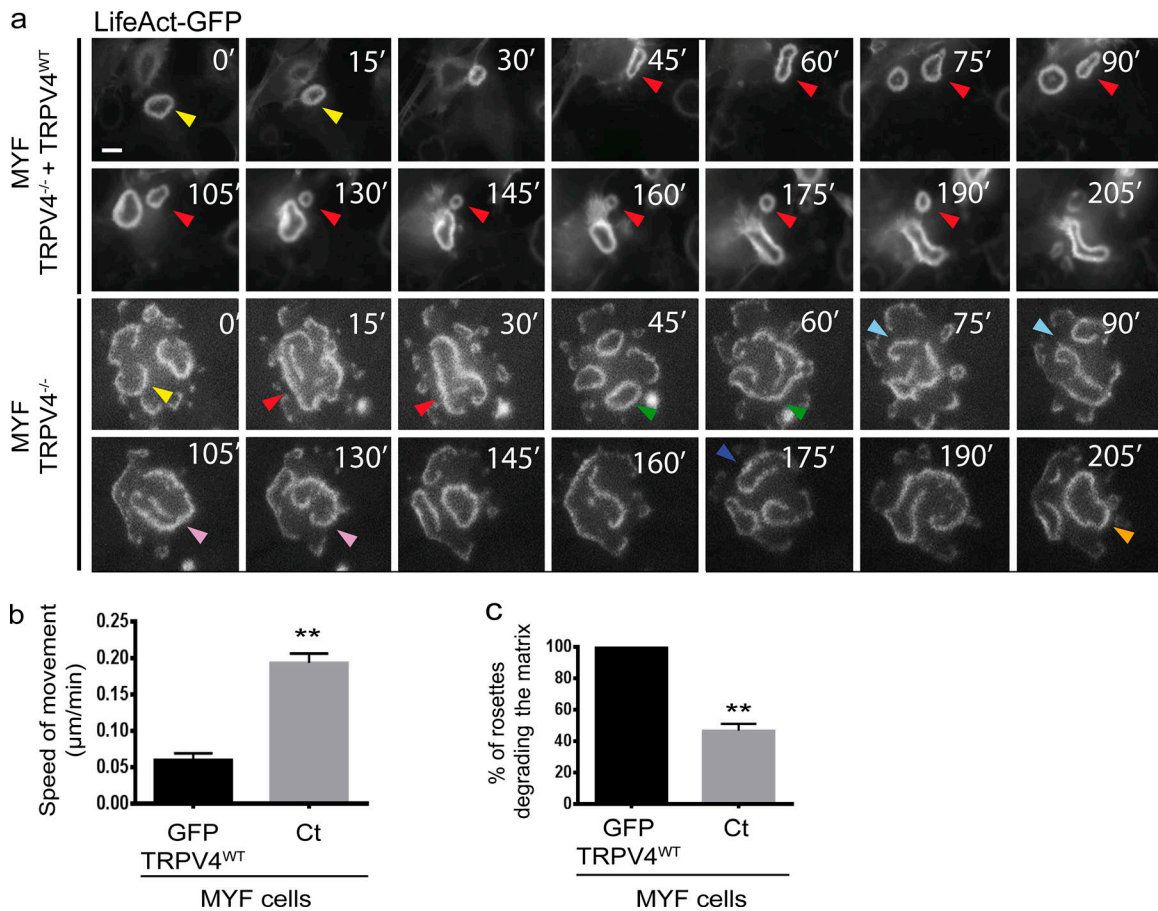


Figure S2. **TRPV4 regulates the dynamics of the acto-adhesive functions of invadosomes and their ability to digest ECM.** (a) Representative images extracted from a time series of MYF-TRPV4^{-/-} cells expressing LifeAct-GFP with or without TgRFP-TRPV4^{WT}. In the absence of TRPV4, invadosomes exhibited a high rate of turnover (multicolored arrowheads), whereas the rescued expression of TgRFP-TRPV4^{WT} induced long-lasting and less dynamic rings (red arrowheads). (b) Quantification of the average speed of invadosome ring formation in MYF cells expressing LifeAct-RFP with or without GFP-TRPV4^{WT} (SEM; *n* = 3; >25 rings per condition; unpaired *t* test). (c) Quantification of the percentage of invadosomes in MYF cells that do or do not express GFP-TRPV4^{WT} directly associated with the degradation of gelatin-Alexa Fluor 647 (SEM; *n* = 3; >70 rings per condition; unpaired *t* test). *, *P* ≤ 0.05; **, *P* ≤ 0.01; ***, *P* ≤ 0.001; ****, *P* ≤ 0.0001. Scale bar: 2 µm (a).

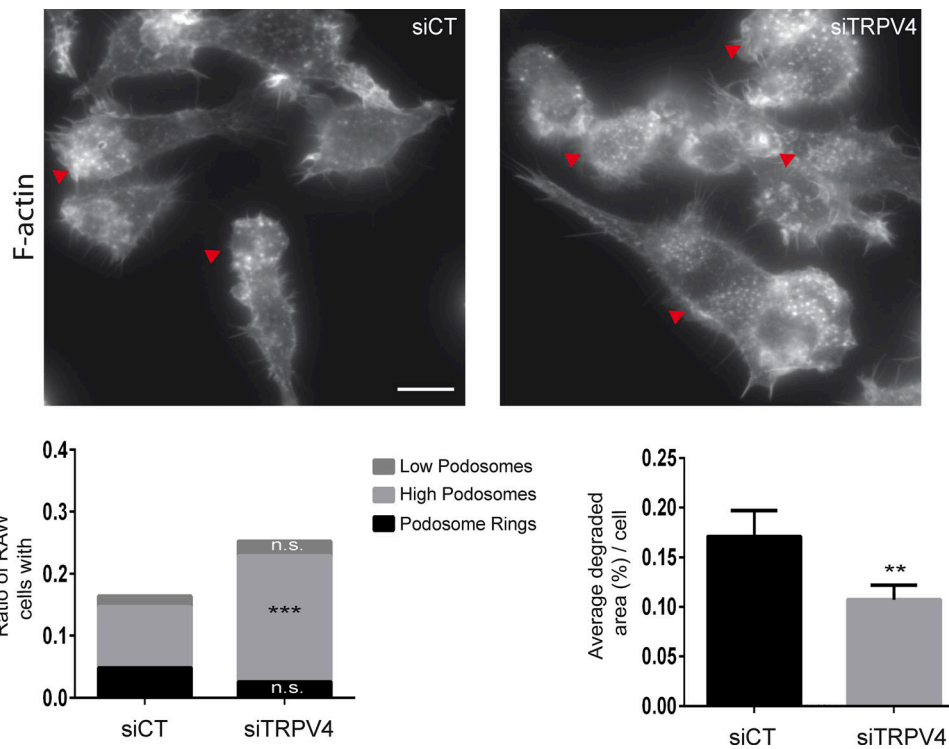


Figure S3. **TRPV4 is also a regulator of ADC in podosomes of the macrophage cell line RAW264.7.** Representative images of the RAW264.7 cell line in which podosomes (red arrows) are visualized by phalloidin-TRITC staining and treated with control or TRPV4 siRNA. TRPV4 silencing induced a significant increase in the number of macrophages forming a high number of podosomes (SEM; $n = 3$; >200 cells per condition; unpaired t test) and a decrease in the average degradation area per cell (SEM; $n = 2$; >40 cells per condition; unpaired t test). *, $P \leq 0.05$; **, $P \leq 0.01$; ***, $P \leq 0.001$. Scale bar: 5 μm . n.s., not significant.

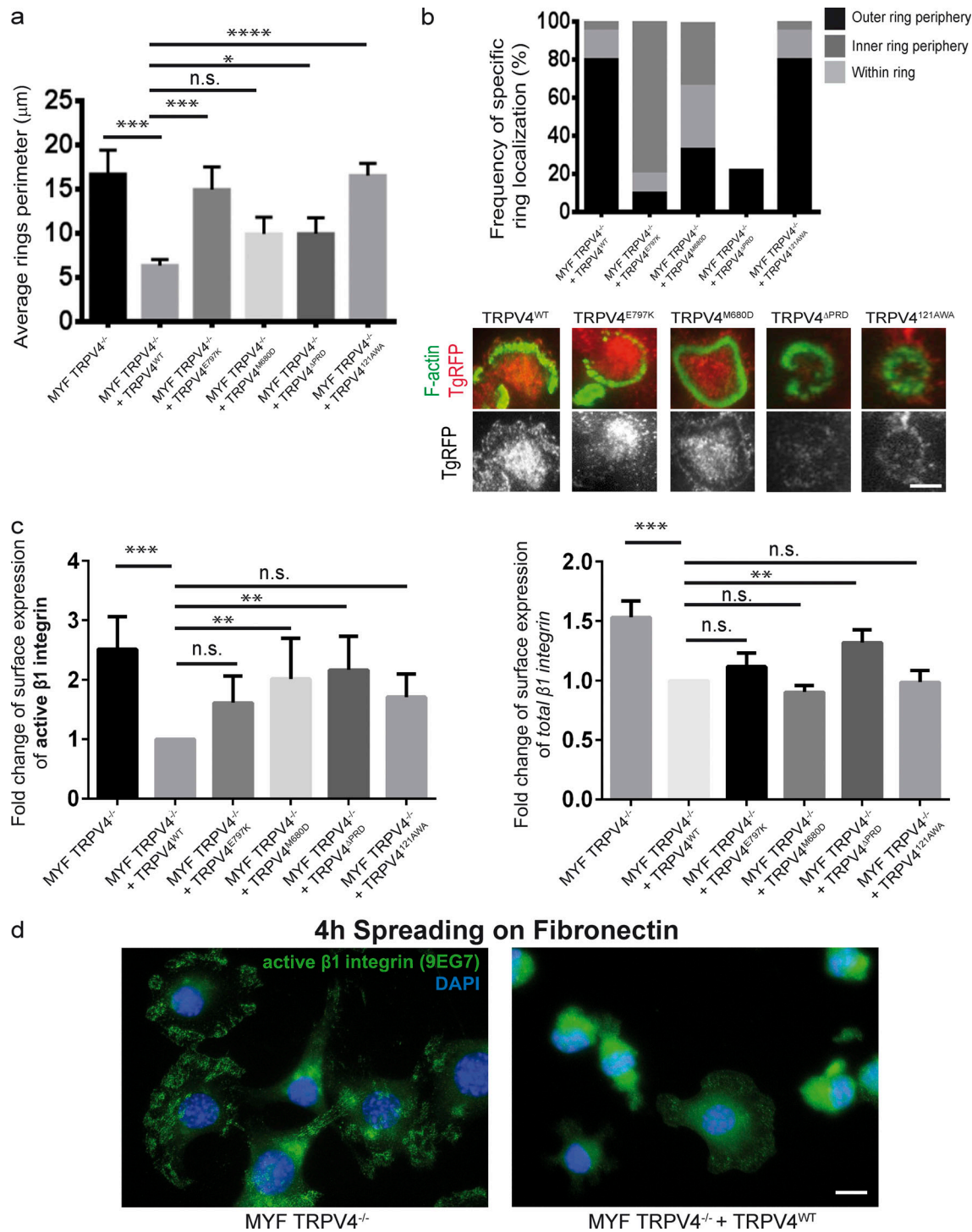


Figure S4. **Structure–function studies revealed the importance of calcium permeation and the adaptor functions of TRPV4 on TRPV4 localization and its regulation of invadosomes.** (a) Quantification of the diameter of invadosome rings in MYF-TRPV4^{-/-} cells expressing TgRFP-TRPV4^{WT} and the indicated TgRFP-TRPV4 mutants (SEM; $n = 3$; >35 rings per condition; unpaired t test). (b) Quantification of the percentage of invadosome rings that accumulated TgRFP-TRPV4^{WT} or the indicated TgRFP-TRPV4 mutants (expressed in MYF-TRPV4^{-/-} cells) mostly at the outer rim, at the inner rim, or directly inside invadosomes (SE; $n = 3$; >40 rings per condition; unpaired t test). This quantification was associated with representative images of MYF-TRPV4^{-/-} cells stably expressing TgRFP-TRPV4^{WT} or the indicated TgRFP-TRPV4 mutant stained with phalloidin-Alexa Fluor. (c) Quantification of the fold change of the normalized values (on the values of MYF-TRPV4^{-/-} cells expressing TgRFP-TRPV4^{WT}) of the mean intensity per cell of either active β1-integrin (Ab 9EG7) or total β1-integrins (Ab Mb1-2) in MYF-TRPV4^{-/-} cells rescued with indicated TRPV4 mutants or not. Reexpression of TgRFP-TRPV4^{WT} induced a significant decrease in β1-integrin activation (SEM; $n = 3–6$; >8,000 cells per condition; unpaired t test). (d) Representative epifluorescence images of MYF-TRPV4^{-/-} cells stably expressing or not TgRFP-TRPV4^{WT}, stained with DAPI (blue) and active β1-integrin (9EG7–Alexa Fluor 488) and shortly spread (4 h) on the β1-integrin–ligand fibronectin (10 µg/ml). MYF-TRPV4^{-/-} cells spread and assembled active β1-integrin structures faster than when reexpressing TgRFP-TRPV4^{WT}. *, $P \leq 0.05$; **, $P \leq 0.01$; ***, $P \leq 0.001$; ****, $P \leq 0.0001$. Scale bars: 4 µm (b), 8 µm (d). n.s., not significant.

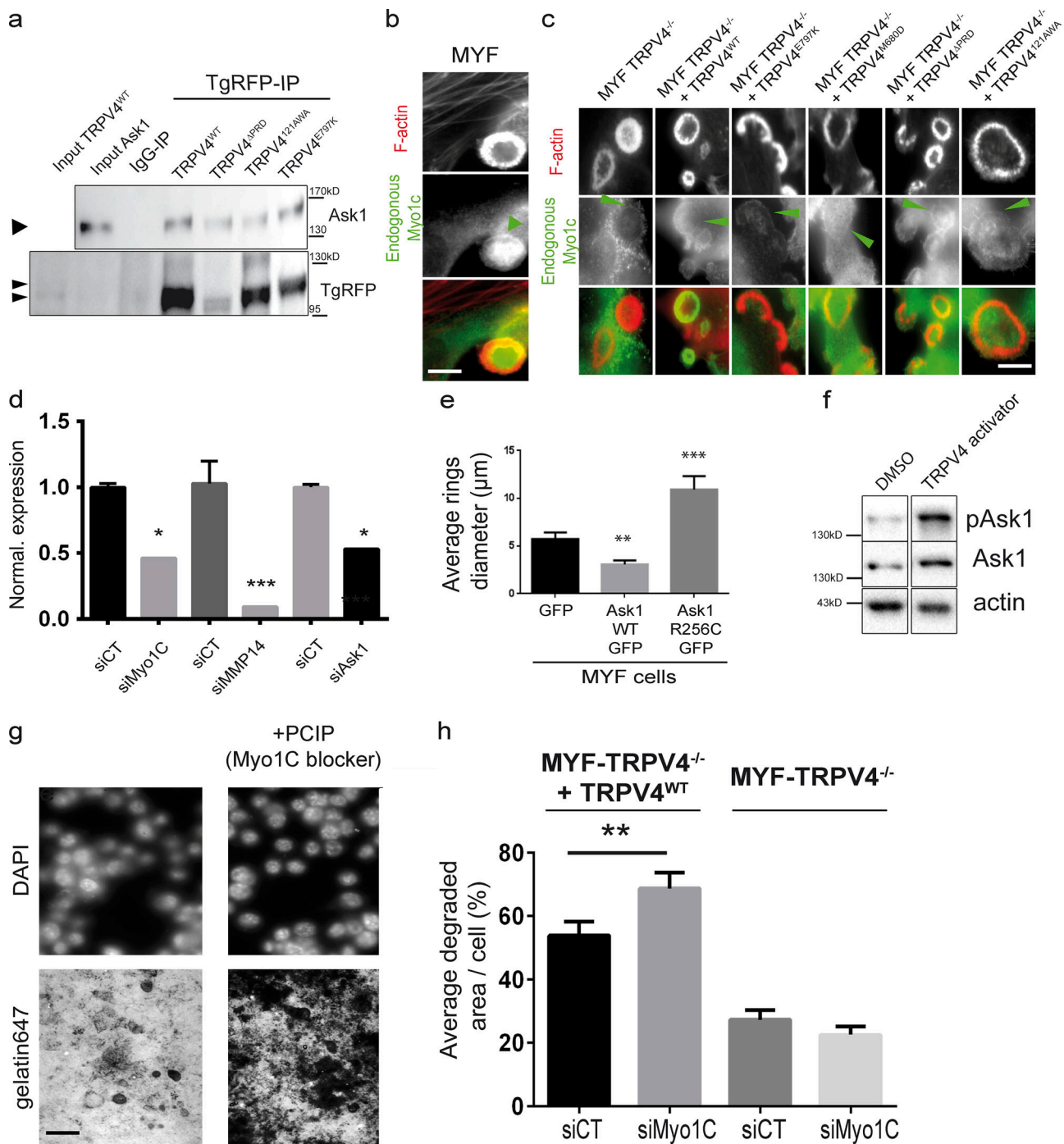


Figure S5. Characterization of the effects of ASK1 and MYO1C on invadosomes. (a) The coIP of Flag-ASK1 and TgRFP-TRPV4^{WT} (appearing as doublet, double black arrowhead) or the indicated TgRFP-TRPV4 mutant overexpressed in HEK293 cells with tGFP antibody confirmed the specific interaction between these two proteins independently of the different TRPV4-functions modified by mutation. (b) Representative epifluorescence images of MYF cells stained for F-actin (phalloidin-Alexa Fluor 647) and endogenous MYO1C (M3567 antibody). The green arrowhead indicates MYO1C accumulation at the invadosome periphery. (c) Representative epifluorescence images of MYF-TRPV4^{-/-} cells stably expressing or not TgRFP-TRPV4^{WT} or indicated mutants, stained for F-actin (phalloidin-Alexa Fluor 647) and endogenous MYO1C. In each case, MYO1C is globally observed at the periphery of the invadosome (green arrows). (d) Quantification of the efficiency of different siRNA treatments by qPCR (SEM; n = 3; unpaired t test). (e) Quantification of the thickness of invadosome rings in MYF cells expressing control plasmid (GFP), ASK1-Flag, or the kinase dead mutant ASK1^{R256C}-Flag (SEM; n = 3; >25 rings per condition; unpaired t test). (f) Treatment of HEK cells transfected with ASK1-Flag and tGFP-TRPV4^{WT} with DMSO or the specific TRPV4 activator GSK1016790A (100 nM) for 15 min induced the specific activation of ASK1; observed by Western blotting P-T845ASK1, total ASK1, and actin. (g) Representative images of MYF cells treated with DMSO or the specific MYO1C inhibitor PCIP (used at 100 μM) for 14 h after being spread on digestible gelatin-Alexa Fluor 647. The cell number was quantified through DAPI staining. (h) Quantification of the average degradation area per cell of MYF-TRPV4^{-/-} cells rescued with tGFP-TRPV4^{WT} treated with the indicated siRNA. The ability of MYO1C silencing to increase degradation appears dependent on the expression of TRPV4 (SEM; n = 3; >80 cells per condition; unpaired t test). *, P ≤ 0.05; **, P ≤ 0.01; ***, P ≤ 0.001. Scale bar: 10 μm (b and c), 10 μm (g).

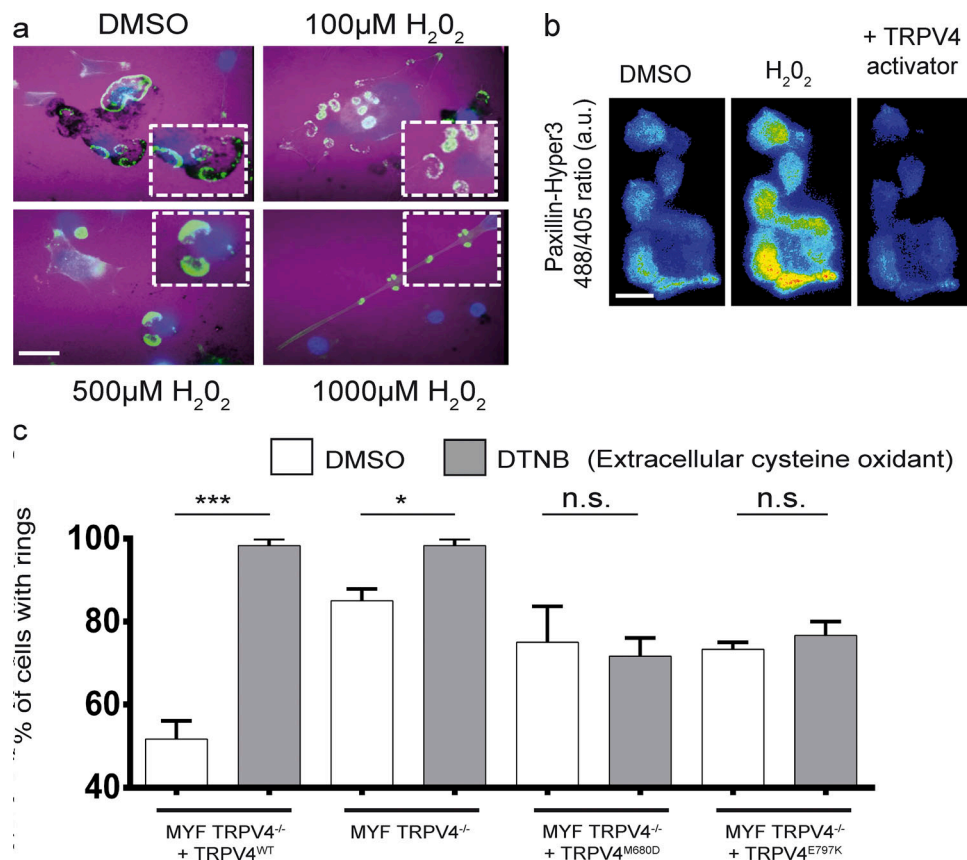


Figure S6. **Invadosome responses to the cell-permeable oxidant H₂O₂ and the extracellular oxidant DTNB.** (a) Representative images of invadosomes (zoom of invadosome rings in dashed boxes) in MYF cells treated with increasing doses of H₂O₂ and DMSO for 6 h (stained with phalloidin–Alexa Fluor 488 and DAPI) after being spread on digestible gelatin-647. (b) Representative images extracted from a time series of MYF cells expressing paxillin-Hyper3 that exhibited an increase in the 488 nm/405 nm ratio in response to H₂O₂ addition (50 μM for 5 min), which then decreased after the addition of the TRPV4 activator GSK1016790A (100 nM for 5 min). (c) Quantification of the percentage of cells with invadosome rings in MYF-TRPV4^{-/-} cells that were or were not rescued with TgRFP-TRPV4^{WT}, the permeation mutant TgRFP-TRPV4^{M680D}, and the disease-associated mutant TgRFP-TRPV4^{E797K} treated with the extracellular oxidant DTNB at 4 μM for 1 h (SEM; n = 3; >150 cells per condition; unpaired t test). *, P ≤ 0.05; **, P ≤ 0.01; ***, P ≤ 0.001. Scale bars: 10 μm (a), 4 μm (b). n.s., not significant.

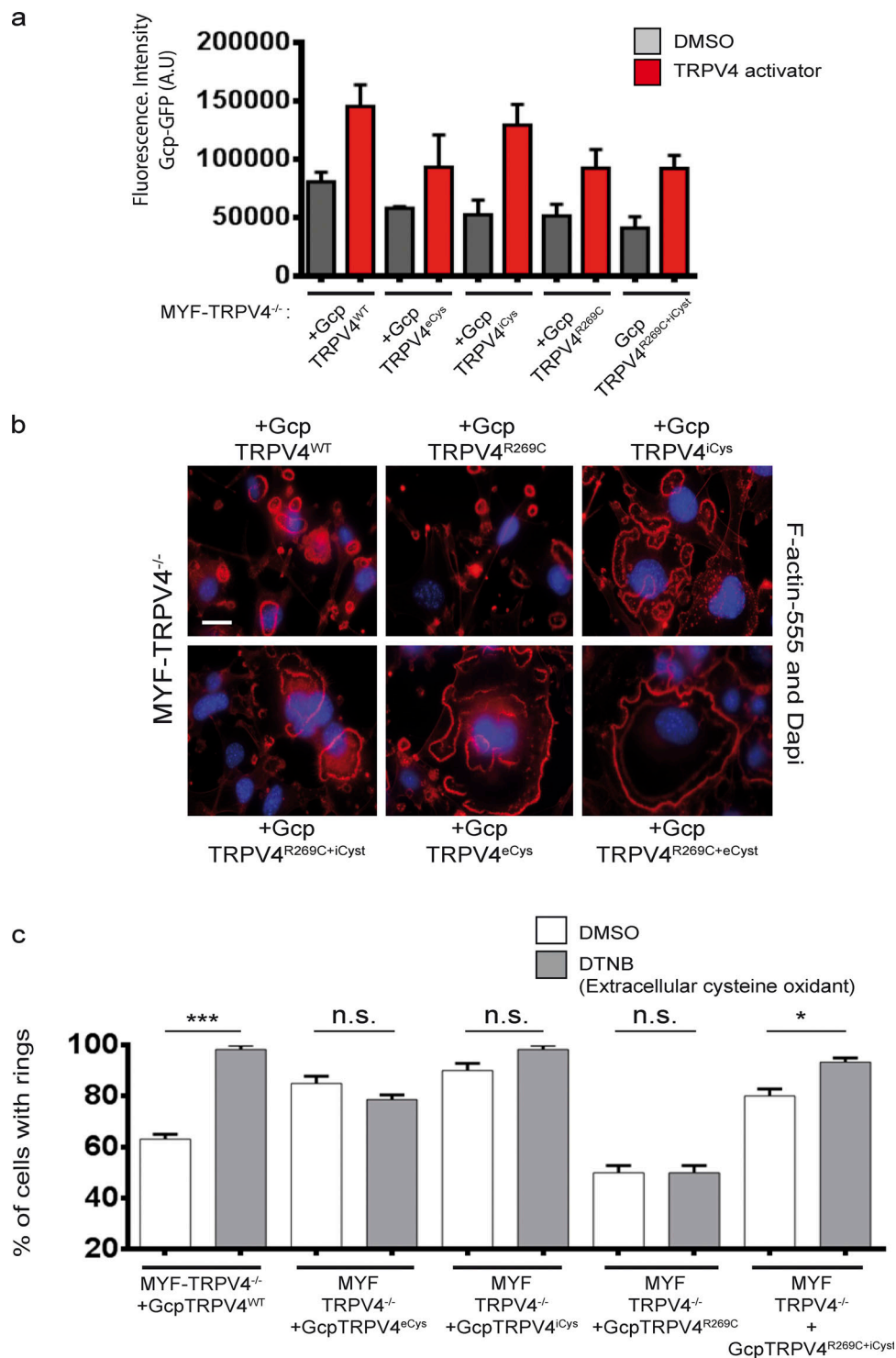


Figure S7. **Characterization of Gcamp-TRPV4^{WT} and Gcamp-TRPV4 mutants of extra- and intracellular stretches of cysteines that rescue the activity of a pathological cysteine mutation (TRPV4^{R269C}).** (a) FACS analysis of the fluorescence intensity of the Gcamp signal in MYF-TRPV4^{-/-} cells rescued with Gcamp-TRPV4^{WT} or the indicated Gcamp-TRPV4 mutants affecting disulfide bridge formation (SEM; $n = 3$; >10,000 cells per condition; unpaired t test). (b) Representative images of invadosomes in MYF-TRPV4^{-/-} cells (stained with phalloidin-Alexa Fluor 488 and DAPI) rescued with Gcamp-TRPV4^{WT} or the indicated Gcamp-TRPV4 mutants affecting disulfide bridge formation. (c) Quantification of the percentage of cells with invadosome rings in MYF-TRPV4^{-/-} cells rescued with Gcamp-TRPV4^{WT} or the indicated Gcamp-TRPV4 mutants affecting disulfide bridge formation, treated with the extracellular oxidant DTNB at 4 μ M for 1 h (SEM; $n = 3$; >150 cells per condition; unpaired t test). *, $P \leq 0.05$; **, $P \leq 0.01$; ***, $P \leq 0.001$. Scale bar: 10 μ m (b). n.s., not significant.

Provided online is Data S1, an Excel dataset that describes the constructs, siRNA mixes, and antibodies used in this study.